# Using the Hess Adaptive Pilot Model for Modeling Human Operator's Control Adaptations in Pursuit Tracking

Jakimovska, N.; Pool, D.M.; van Paassen, M.M.; Mulder, Max

**DOI**
10.2514/6.2023-0541

**Publication date**
2023

**Document Version**
Final published version

**Published in**
AIAA SciTech Forum 2023

AIAA SciTech Forum
23-27 January 2023, National Harbor, MD & Online
AIAA SCITECH 2023 Forum

10.2514/6.2023-0541

# Using the Hess Adaptive Pilot Model for Modeling Human Operator's Control Adaptations in Pursuit Tracking

Nora Jakimovska*, Daan M. Pool†, Marinus M. van Paassen‡ and Max Mulder§
*Delft University of Technology, Delft, Zuid-Holland, The Netherlands*

**An improved understanding of pilot's control behavior adaptations in response to sudden changes in the vehicle dynamics is essential for realizing adaptive support systems that remain effective when task characteristics suddenly change. In this paper, we replicate, extend, and validate the 'adaptive pilot model' proposed by Hess to verify its effectiveness for predicting human adaptive behavior in pursuit tracking tasks. The model relies on a Triggering function, that compares the current tracking performance to a stored nominal (pre-transition) state, and an Adaptation mechanism which determines new adapted human operator gain settings proportional to the magnitude of the off-nominal error occurrences. For model validation data from a previous experiment were used, where ten participants performed a pursuit tracking task with transitions in controlled element dynamics from a single to a double integrator, and vice versa. Overall, with an added human operator delay and participant-specific inner- and outer-loop gain adjustments, the model was found to accurately describe the measured steady-state tracking behavior for the participants in our data set. The results for the time-varying single integrator to double integrator transitions showed that the model can capture the transient control behavior of participants. However, the adaptive logic could only be tuned to activate for participants that had a pre-transition crossover frequency above 0.9 rad/s. Furthermore, the model was not able to capture the change in control behavior for transitions from a double to a single integrator. Here, as no distinct degradation in tracking performance occurs for such a transition to a more easily controlled system, the model's proposed Triggering logic will not activate. Further investigation and more experiment data are required for improving the applicability of the model's adaptive logic and to enable more accurate prediction of adaptive human control behavior.**



## Nomenclature

| | | | |
|---|---|---|---|
| $A_n$ | Amplitude of the $n^{\text{th}}$ forcing function sine, rad | $k_c(t)$ | Controlled element gain |
| $C$ | Target forcing function signal, rad | $K_p$ | Outer-loop position gain |
| $e$ | Tracking error signal, rad | $K_{trigger}$ | Binary triggering variable |
| $f_t$ | Target forcing function signal, rad | $K_r$ | Inner-loop rate gain, s |
| $G$ | Maximum rate of change, $s^{-1}$ | $M$ | Output of system, rad |
| $G_{nm}(s)$ | Neuromuscular dynamics transfer function | $M$ | Sigmoid maximum rate of change, s |
| $H(s)$ | Second-order low-pass filter on $x$ signal | $\dot{M}$ | Output rate of system, $s^{-1}$ |
| $H_{del}(s)$ | Human operator delay transfer function | $N$ | Number of controlled axes |
| $I(s)$ | Second-order low-pass filter on $X_n$ signal | $n$ | Sinusoid index |
| $J(s)$ | Second-order low-pass filter on adaptive gains | $R$ | Input of outer-loop signal |
| $K$ | Number of samples | $t$ | Time, s |
| $K_{a_p}$ | Adaptation constant for $K_p$ gain | $t_c$ | Time of change in controlled element, s |
| $K_{a_r}$ | Adaptation constant for $K_r$ gain, s | $T_m$ | Measurement time, s |

*M.Sc. student, Control and Simulation section, Faculty of Aerospace Engineering, P.O. Box 5058, 2600GB Delft, The Netherlands; n.jakimovska@student.tudelft.nl.

†Assistant Professor, Control and Simulation section, Faculty of Aerospace Engineering, P.O. Box 5058, 2600GB Delft, The Netherlands; d.m.pool@tudelft.nl. Associate Fellow AIAA.

‡Associate Professor, Control and Simulation section, Faculty of Aerospace Engineering, P.O. Box 5058, 2600GB Delft, The Netherlands; m.m.vanpaassen@tudelft.nl. Member AIAA.

§Professor, Control and Simulation section, Faculty of Aerospace Engineering, P.O. Box 5058, 2600GB Delft, The Netherlands; m.mulder@tudelft.nl. Associate Fellow AIAA.

| | |
|---|---|
| $T_r$ | Reaction time, s |
| $t_s$ | Simulation transient time window, s |
| $u$ | Human operator control output signal, rad |
| $u_h$ | Measured control output, rad |
| $u_m$ | Model control output, rad |
| $x$ | Hess model triggering signal, rad$^2$ |
| $X_n$ | Hess model strength of adaptation signal |
| $Y_c(s)$ | Controlled dynamics transfer function |
| $Y_p(s)$ | Human operator transfer function |
| $\Delta K_p$ | Outer-loop gain $K_p$ increment |
| $\Delta K_r$ | Inner-loop gain $K_r$ increment, s |
| $\zeta_{lp}$ | Low-pass filter damping ratio |
| $\zeta_{nm}$ | Neuromuscular damping ratio |
| $\Theta$ | Parameter vector |
| $\tau_e$ | Human time-delay, s |
| $\phi_m$ | Phase margin, deg |
| $\phi_n$ | Phase of the $n^{\text{th}}$ forcing function sine , rad |
| $\omega_b(t)$ | Time-varying pole of the controlled element, rad/s |
| $\omega_c$ | Crossover frequency, rad/s |
| $\omega_{lp}$ | Low-pass filter frequency, rad/s |
| $\omega_m$ | Fundamental measurement frequency, rad/s |
| $\omega_n$ | Frequency of the $n^{\text{th}}$ forcing function sine, rad/s |
| $\omega_{nm}$ | Neuromuscular frequency, rad/s |

*Abbreviations*

| | |
|---|---|
| CE | Controlled element |
| rms | root mean square |
| VAF | variance accounted for |



# I. Introduction

As controllers, humans have unique adaptive behavior capabilities, which allow them to lessen the effects of any incidents [1–10]. Understanding how pilots adapt their control strategy to maintain stability has several advantages. Technologies such as autopilots and automatic landing systems rely on the pilot's adaptive capabilities to quickly adjust their control strategies when detecting failures. Therefore, modeling human's adaptive behaviour does not only improve automation, but may improve training procedures and in turn increase safety in aviation.

While several researchers have investigated human controllers' adaptive behavior, mostly in response to changes in the controlled vehicle's dynamics [1–3, 5–7, 10–16], a solid and practical theoretical modeling framework on what triggers human adaptation is still lacking. Especially for *pursuit* tracking tasks, we miss a more thorough understanding of which (off-nominal) characteristics of which control task signals observed by human controllers may trigger adaptation, how human controllers determine an effective adaptation of their control dynamics, and how this should be captured in an adaptive pilot model for pursuit tracking.

To address this gap, this paper will present the results of a study where the 'adaptive pilot model' framework proposed by Hess [6] is matched to the time-varying pursuit tracking task data collected by Terenzi et al. [10] in a recent human-in-the-loop experiment performed at TU Delft. Hess' adaptive pilot includes a mathematical framework that predicts when pilots may *trigger* an adaptation of their control behavior, as well as predicting a realistic *adaptation* of pilot control gains.

In this paper, we will first replicate the adaptive pilot model simulation results reported by Hess [6] to verify our model implementation. Then, we will implement a number of key adjustments to the model (e.g., add a human operator delay) to ensure it can be fitted to the data from [10]. Finally, using parameter sensitivity analyses, we will show to what extent key parameters of the models Triggering and/or Adaptation logic may need to be adapted to model the behavior of different human operators in our experiment data set. Ultimately, the goal of this paper is bring us closer to a complete model of time-varying human adaptive behavior to changes in control task variables and the environment.

The structure of this paper is as follows. Section II presents a detailed description of the adaptive pilot model proposed by Hess and our proposed updates to the model's structure. Additionally, we present the results from replicating the original model and results presented in [6]. In Section III, the key details of the experiment data set from [10] are provided, as well as an overview of the steps used to fit and analyse the adaptive pilot model are presented. The obtained model fitting and validation results are presented in Section IV. Finally, the paper ends with a discussion (Section V) and the main conclusions (Section VI).

# II. Hess Adaptive Pilot Model

## A. Model Structure

We study the "adaptive pilot model" proposed by Hess [6], see Fig. 1, for modeling human controller adaptation to changes in the CE dynamics in pursuit tracking. The model's block diagram in Fig. 1 has been adapted compared to [6]

to explicitly separate the "Triggering" and "Adaptation" actions of the model's adaptive logic. Furthermore, the original model as described by Hess [6] does not include a human operator time delay, which is essential for matching the model to the experiment data from Terenzi et al. [10]. Hence, in this paper we add a time delay to the adaptive pilot model, as indicated with the $H_{del}$ block shown in red in Fig. 1. As in our experiments we always ensure no manipulator limits are reached, in this paper the model's input saturation block (shown with a dashed outline) is not considered in our analysis.

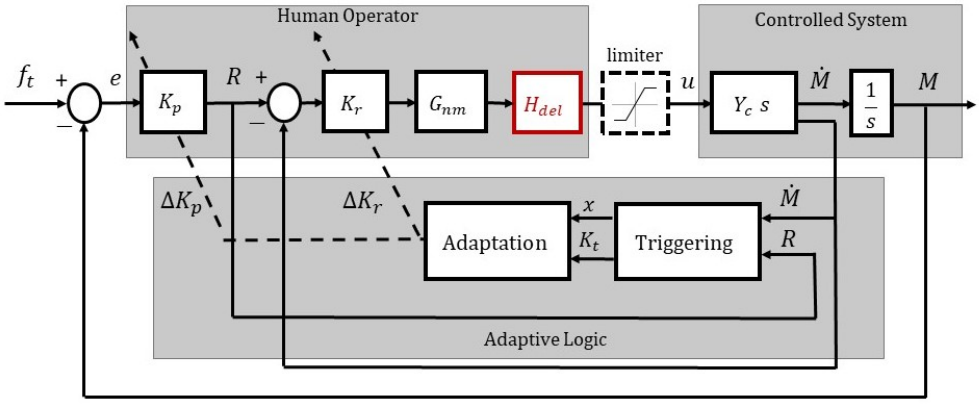


**Fig. 1 Block diagram of the Hess adaptive pilot model, showing its three main parts as gray shaded boxes; the Human operator dynamics, the Controlled system dynamics, and the Adaptive Logic. In the first step of the Adaptive logic, Triggering, the signals $\dot{M}$ and $R$ are used as inputs to obtain the $x(t)$ signal as well as the output of the trigger function $K_{trigger}$. These are then used in the second step, Adaptation, to update the Human operator control gains($K_p$, $K_r$) depending on if $K_{trigger}$ is activated.**

In Fig. 1, the symbol $Y_c$ indicates the controlled element (CE) dynamics. To implement an outer $M$ loop, as well as an inner $\dot{M}$ loop, $Y_c$ is implemented with a separated integrator, as shown in the '*Controlled System*' block in Fig. 1. The remaining blocks in Fig. 1 together represent the adaptive human operator control dynamics. First, the '*Human Operator*' block includes the human operator's outer- (position) and inner-loop (rate) control gains, $K_p$ and $K_r$, respectively. In the model, $K_p$ controls the proportional control performed by the human operator, while $K_r$ defines the magnitude of the rate feedback, i.e., human operator 'lead' [8, 17]. Additionally, human operator limitations are included in the form of an added time delay $\tau_e$, i.e., $H_{del} = e^{-\tau_e s}$, and the human operator's neuromuscular dynamics $G_{nm}$, representing the dynamics of the operator's limb-manipulator interaction, modeled as a second-order mass-spring-damper system:

$$G_{nm}(s) = \frac{\omega_{nm}^2}{s^2 + 2\zeta_{nm}\omega_{nm}s + \omega_{nm}^2}, \tag{1}$$

where [6] implements constant representative values for the neuromuscular system model's parameters: $\omega_{nm}$ = 10 rad/s and $\zeta_{nm}$ = 0.707.

*1. Adaptive Logic: Triggering*

Fig. 1 shows that the adaptation of the human operator is represented through the '*Adaptive Logic*' which is divided into two sequential steps, namely: 'Triggering' and 'Adaptation'. The first step, Triggering, models how a human operator may detect a change in the controlled element dynamics. For this, Hess [6] proposes that the human operator uses a signal proportional to the inner-loop tracking error. In mathematical terms this is denoted as the signal $x$, which is a low-pass filtered signal based on the sign and magnitude of the error in the inner loop ($R - \dot{M}$), and is calculated using Eq. (2)-(4) [6]:

$$x^*(t) = \text{sgn}\{|R(t)| - |\dot{M}(t)|\} \cdot [|R(t)| - |\dot{M}(t)|]^2 \tag{2}$$

$$X(s) = X^*(s) \cdot H(s) \tag{3}$$

$$H(s) = \frac{\omega_{lp}^2}{s^2 + 2\zeta_{lp}\omega_{lp}s + \omega_{lp}^2} \tag{4}$$

It should be noted that the $x^*(t)$ signal of Eq. (2) is not used in [6], but is introduced to represent the 'unfiltered' $x$ signal. As indicated in Eq. (3), this $x^*$ signal is filtered using a second-order low-pass filter $H(s)$, which introduces smoothing and lag in the Triggering process, to obtain the same $x$ signal defined by Hess. The second-order low-pass filter $H(s)$ is defined in Eq. (4). In [6], $\zeta_{lp} = 1$ and $\omega_{lp} = 1.5$ rad/s are used as the settings for $H(s)$.

When the $x$ signal becomes exceedingly large in magnitude, a different control gain setting is needed and hence the model's Triggering mechanism should be activated, which as proposed in [6] is implemented through the following equation and the $K_{trigger}$ signal of Fig. 1:

$$K_{trigger}(t) = \begin{cases} 1 & \text{if the instantaneous value of } \sqrt{|x|} \geq 3 \cdot \text{rms}[\sqrt{|x|}] \text{ and } t \geq t_s \\ 0 & \text{if the instantaneous value of } \sqrt{|x|} < 3 \cdot \text{rms}[\sqrt{|x|}] \text{ or } t < t_c \end{cases} \tag{5}$$

In Eq. (5), the square root of $x$, ($\sqrt{|x|}$), is used because the square of the error signal is used to obtain $x$, see Eq. (2). Moreover, the expression $3 \cdot \text{rms}[\sqrt{|x|}]$ represents the 'Triggering limit', where the factor of 3 defines the lower limit of a deviating error pattern that would induce the human pilot to adapt.

In Eq. (5), the additional time-dependent terms were added to the Triggering logic in [6] to suppress potential artifacts in the Triggering model. Both these terms are thus not directly representative for real human operators' adaptive behavior. For example, by only triggering for $t \geq t_s$ (with $t_s = 10$ s [6]) potential effects of initial model simulation transients were suppressed. Second, by not allowing the model to trigger for $t < t_c$, where $t_c$ indicates the time at which the CE dynamics transition, any false positive detections prior to the CE change are suppressed.

*2. Adaptive Logic: Adaptation*

When the model's adaptive logic is triggered (i.e., $K_{trigger} = 1$), then new appropriate gains $K_p$ and $K_r$ are determined in the 'Adaptation' step of the adaptive pilot model, see Fig. 1. As proposed in [6], the primary adaptive change of the inner-loop gain $K_r$ is determined using the following equation:

$$\Delta K_r(t) = X_n(t) \cdot K_{a_r} \cdot K_{\text{trigger}}(t) \tag{6}$$

Eq. (6) shows that changes to the $K_r$ gain only occur when the Triggering occurs, i.e., $K_{trigger} = 1$. Furthermore, the magnitude of the gain adjustment is directly controlled by the adaptation gain $K_{a_r}$ (set to unity in [6]) and the $X_n(t)$ signal, which is defined as follows [6]:

$$X_n(t) = \frac{x(t)}{\text{rms}(R^2)} \cdot \frac{1}{N} \tag{7}$$

Eq. (7) shows that $X_n$ is calculated from $x$ by normalizing with $\text{rms}(R^2)$, which is done to ensure that the adaptation is not dependent on the numerical magnitude of control-loop signals (e.g., invariant to changes in the magnitude of the forcing function $f_t$). The root mean square (rms) value of $R^2$ is chosen because it is also used in the calculation of the $x$ signal. In the model, the $\text{rms}(R^2)$ term is considered a constant in time-varying cases, and its value is calculated from the steady-state pre-transition system. The variable $N$ represents the number of axes that are controlled by the human operator [6]. This variable results in a less aggressive control behavior in multi-axis tasks compared to controlling a single axis. In this paper, only a single-axis is considered, so $N = 1$.

Finally, in [6] both the $X_n$ signal of Eq. (7) and $\Delta K_r$ as defined in Eq. (6) were filtered using a second-order low-pass filter equivalent to Eq. (4), with $\omega_{lp} = 1$ rad/s and $\zeta_{lp} = 1$. Here, we refer to these two filters as $I(s)$ and $J(s)$, respectively. As in our implementation of the model for describing the experiment data of [10] the use of two filters was found to be superfluous, only the filter on $\Delta K_r$ was retained:

$$J(s) = \frac{\omega_{lp}^2}{s^2 + 2\zeta_{lp}\omega_{lp}s + \omega_{lp}^2} \tag{8}$$

An example of how this "Adaptation" process works is shown in Fig. 2, where the $K_{trigger}$, $X_n$, and $\Delta K_r$ signals are shown. For $\Delta K_r$ the direct result of Eq. (6) is shown, before the $J(s)$ filter is applied and with $K_{a_r} = 1$. Fig. 2 shows that during the time that the Triggering is active, the gain adjustment is directly proportional to the $X_n$ signal. This continues until the gain adjustment is successful in stabilizing the control loop, which will cause the Triggering to stop. The value of $\Delta K_r$ is from that point on kept at the final adapted setting, until the next Triggering activation.

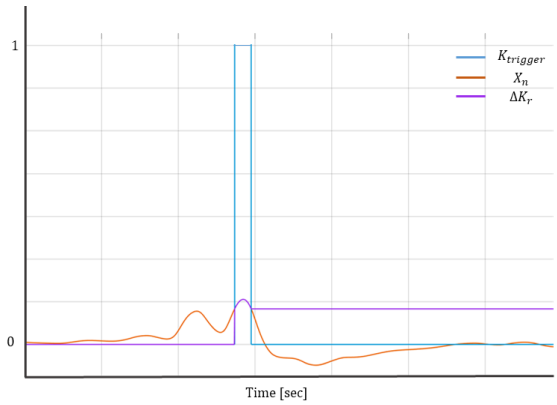


**Fig. 2 Example of how the adaptive pilot model's "Triggering" signals drive human operator gain adaptation.**



To complete the adaptation of the human operator model, the corresponding change in the outer-loop gain $K_p$ is calculated using the following equation [6]:

$$\Delta K_p(t) = \begin{cases} \Delta K_r(t) \cdot K_{a_p} & \text{if } \Delta K_r(t) > 0 \\ 0 & \text{if } \Delta K_r(t) \leq 0 \end{cases} \tag{9}$$

where $K_{a_p}$ again is an adaptation gain that needs to be tuned for the outer-loop control adaptation. As shown by Eq. (9), the adaptation of the outer-loop gain $K_p$ is directly linked to the change in the inner-loop gain $K_r$. In [6], where both gains were required to increase for the studied CE transitions, the scaling factor between both gain adjustments $K_{a_p} = 0.35$. Furthermore, as indicated with the two cases in Eq. (9), in [6] the $K_p$ gain was restricted from changing in case $\Delta K_r < 0$. Based on the $\Delta K_r$ and $\Delta K_p$ signals, the adapted operator gain values at time $t$ are calculated as:

$$\begin{aligned} K_r(t) &= \Delta K_r(t) + K_r(0) \\ K_p(t) &= \Delta K_p(t) + K_p(0) \end{aligned} \tag{10}$$

where $K_r(0)$ and $K_p(0)$ represent the initial pre-transition reference settings for both human operator gains. Finally, in [6] additional constraints are included on the adapted values of the $K_p$ and $K_r$ gains, see Eq. (11). In this equation, $K_r(0)$ and $K_r(0)$ again represent the initial pre-transition values of $K_p$ and $K_r$ as also used in Eq. (10).

$$\begin{aligned} \left|K_p\right|_{\max} &= 2\left|K_p(0)\right| \\ \left|K_r\right|_{\max} &= 10\left|K_r(0)\right| \end{aligned} \tag{11}$$

### B. Model Implementation Verification

Based on [6] and personal communication with professor Hess, we implemented the adaptive pilot model in Matlab/Simulink. To verify the implementation, we first replicated the simulation results presented in [6]. For this, a single-axis pitch control task was simulated for a total of 120 s, with a change in the CE dynamics occurring at 50 s. Initially, the CE dynamics represented a nominal system $Y_{c,1}(s)$; at 50 s a more challenging dynamics $Y_{c,2}(s)$ was introduced, representing a more difficult to control 'failed' system:

$$Y_{c,1}(s) = \frac{1}{s(s+10)} \qquad Y_{c,2}(s) = \frac{e^{-0.2s}}{s(s+5)(s+10)} \tag{12}$$

Fig. 3 and 4 show direct comparisons between results from [6] and our own implementation's output, for tracking task signals and adaptive operator gains, respectively. The published time trace of the $K_r$ adaptation shows an initial drop in $K_r$ after the induced controlled element change that is not replicated in our model, and is attributed to Simulink simulation setting differences (e.g., integration scheme). For the same reason, our replicated model shows slight differences in the magnitude of the post-failure gain adaptation, which for both $K_p$ and $K_r$ are lower than the results published in [6]. The difference in gain adaptation is relatively small (our final steady-state $K_r$ and $K_p$ differ by factors 1.2 and 0.7, respectively, from [6]), but still affects the post-failure tracking accuracy, as can be observed from Fig. 3. Still, overall we conclude from these figures that a good replication of the results presented by Hess [6] was obtained.

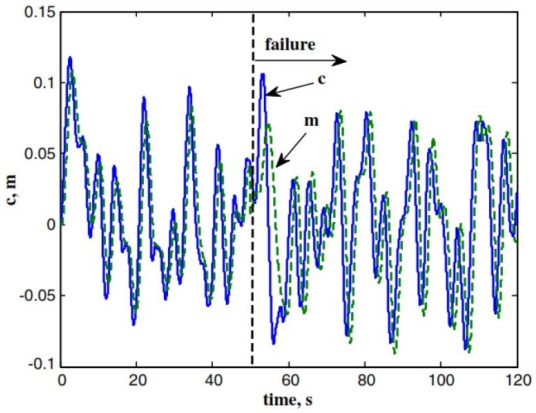


(a) Reference [6]

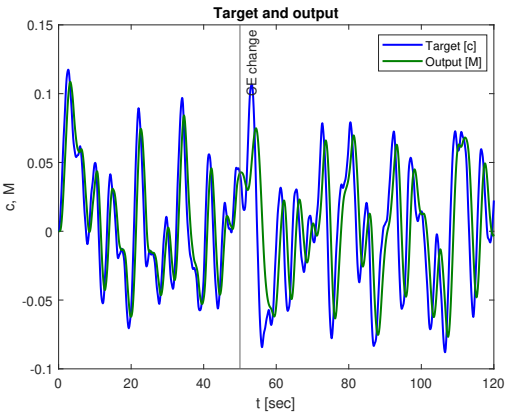


(b) Replicated model

**Fig. 3 Tracking performance as reported in [6] (a) and for our replicated model (b).**

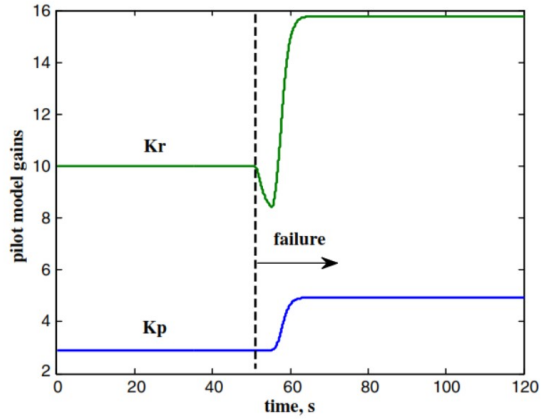


(a) Reference [6]

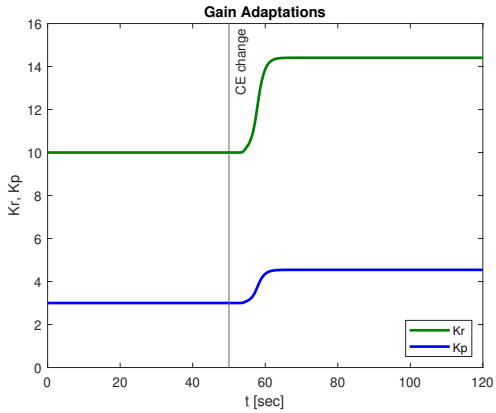


(b) Replicated model

**Fig. 4 Pilot model gain adaptation as reported in [6] (a) and for our replicated model (b).**

### C. Implemented Changes to Model

For matching the adaptive pilot model from [6] with our experimental scenarios from [10], it was found to be necessary to make some modifications to the different parts of the model. The main changes we implemented are listed below, with our motivation for why they were implemented:

1) *Added human operator delay*: As already shown in Fig. 1, a key addition we made to the model is a pure time delay on the modeled human operator response. As it is well-known that human operators in a pursuit tracking task will generally show a latency in their control response equivalent to that seen in compensatory tasks [8, 17], this was found to be a required addition to match the data from the human participants in [10].
2) *Removed saturation on CE input*: As also shown in Fig. 1, the original model implementation included a saturation block on the CE input (human operator control input), to account for potential manipulator constraints. As in the experiment of [10] the manipulator workspace limits were never encountered (by design), the 'limiter' block in Fig. 1 was omitted for our analysis.
3) *Recursive instead of a priori calculation of Triggering limit (rms($\sqrt{|x|}$))*: In [6] it is explained that the root mean square of $\sqrt{|x|}$), which is essential for calculating the $K_{trigger}$ signal in Eq. (5) and defines the Triggering limit, is calculated from "*a trial simulation run with no system changes*" and is thus considered a constant model parameter. In our view, this limit represents the human operator's 'internal model' of the steady-state pre-transition control task [3, 8, 18], which should also be adjusted, long after a CE transition, to a new steady

state. Therefore, we implemented a recursive calculation for $\sqrt{|x|}$): at any time $t$ the full past window from 0 to $t$ is used to calculate $\sqrt{|x|}$) to be used for the calculation of $K_{trigger}$.

4) *Omission of additional time-based constraints on Triggering calculation*: In Eq. (5), additional time-based constraints are implemented in the calculation of the $K_{trigger}$ signal. As this additional logic does not reflect a mechanism that may also be present in real adapting human operators, and may potentially mask sub-optimal functioning of the model's Triggering and Adaptation logic, we have omitted both additional time-based constraints in the model we fit to the data from [10].
5) *Omission of different cases in $\Delta K_p$ calculation*: As shown in Eq. (9), in [6] the update of the outer-loop $K_p$ gain is linked to the current increment of the inner-loop gain $\Delta K_r$, but with some additional constraints that have the following consequences:
    1) When $\Delta K_r > 0$, $\Delta K_p$ must also increase
    2) $\Delta K_p$ always increases by the same constant (0.35) relative to $\Delta K_r$
    3) $K_p$ does not change when $\Delta K_r < 0$, i.e., when $K_r$ is lowered

    As will be shown in Sections IV.A and IV.B, this approach to calculating the updated value of $K_p$ does not match with the expected change of gains for the CE change considered in this paper. For the time-varying scenarios tested in [10], both the $K_r$ and $K_p$ gains are expected to always adapt, independent of whether $K_r$ increases or decreases. Furthermore, with large differences in $K_r$ and $K_p$ between different participants (see Section IV.B), also the relative scaling of the $K_r$ and $K_p$ adaptation would have to be individually set. For this reason, we introduced the adaptation gains $K_{a_r}$ and $K_{a_p}$ in Eq. (6) and (9) to make the gain adjustments, and their relative signs, tunable model parameters.
6) *Addition of 'adaptation gain' parameters and omission of gain adaptation constraints*: Eq. (6) and (9) show that we propose to account for the magnitude of the adaptation of the $K_r$ and $K_p$ gains using additional 'free' model parameters, $K_{a_r}$ and $K_{a_p}$. In our view, this is needed to facilitate tuning the model to different types of CE transitions (for which more or less adaptation may be required), as well as different participants (due to between-subject differences in $K_r$ and $K_p$). Furthermore, as defined in Eq. (11), in [6] constraints are imposed on how much the final gain values can change with respect to their corresponding initial values. In our view, these constraints do not necessarily represent true physical limitations of the human operator. Furthermore, imposing them may mask the true output of the model's adaptive mechanisms. Finally, also the specific multiplier values used in the constraints (2 and 10 for $K_p$ and $K_r$, respectively [6]) would also need to directly adapted to different modeled task settings. Hence, in our fitting of the model to the experiment data of [10] these constraints on the adapted gain values were removed.

# III. Method

## A. Experiment Data

The experiment data used in this paper were obtained from a previous human-in-the-loop experiment performed at TU Delft, as reported in [10]. While the full details of the experiment can be found in the source publication, a selection of important experiment details is repeated here for completeness.

### *1. Control Task*

The control task performed in [10], and considered in this paper, is a pitch attitude pursuit task, as shown in Fig. 5. This pursuit task was, except for the pursuit display, similar to time-varying compensatory control tasks performed in earlier experimental research [7, 15, 18].

### *2. Experiment Conditions*

The experiment of [10] collected human-in-the-loop data for a set of four different experiment conditions, with varying controlled element (CE) dynamics settings, both time-varying and time-invariant. The generic structure of the CE dynamics is defined with the following time-varying transfer function:

$$Y_c(s,t) = \frac{K_c(t)}{s\,(s+\omega_b(t))}, \tag{13}$$

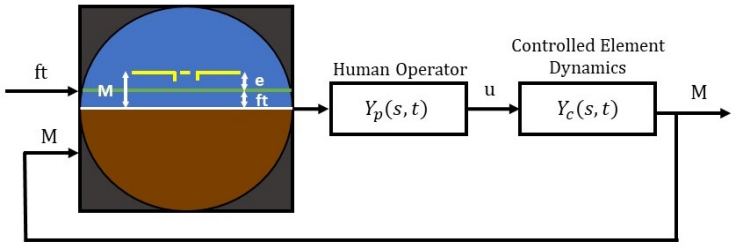


**Fig. 5 Control Task Block Diagram.**

where $K_c$ and $\omega_b$ represent the (potentially time-varying) CE gain and break frequency, respectively. These time-varying parameters are implemented using the following sigmoid function [7]:

$$P(t) = P_1 + \frac{P_2 - P_1}{1 + e^{(-G(t-M))}}, \tag{14}$$

where $P_1$ and $P_2$ represent the initial and final values of the placeholder parameter $P$, i.e., for our CE dynamics $K_c$ or $\omega_b$. The value of $G$ controls the speed of adaptation (steepness of sigmoid), which is kept a constant value of 100 $s^{-1}$ to induce a step-like (instantaneous) CE change [7]. Lastly, the parameter $M$ represents the moment of maximum rate of change (centroid of sigmoid).

As listed in Table 1, Terenzi et al. [10] collected data for two steady-state (time-invariant) conditions, where approximate single-integrator and approximate double-integrator CE dynamics were controlled: DYN1 and DYN2, respectively. Furthermore, data was collected for time-varying transitions, going from single integrator to double integrator and back (DYN121), or vice versa (DYN212). In the experiment of [10], the time-varying tracking runs included two CE transitions at $M_1 = \frac{T_m}{3}$ and $M_2 = \frac{2T_m}{3}$ (see Eq. (14)), where $T_m = 90$ s was the measurement time. However, for the analysis in our current paper the second transition $M_2 = \frac{2T_m}{3}$ is not considered, i.e., we focus on single DYN12 and DYN21 transitions with a tracking run length of 60 s. For the four conditions considered here, the CE parameters are shown in Table 1.

**Table 1 Time-varying controlled dynamics.**

| DYN | $k_{c1}$ [-] | $k_{c2}$ [-] | $\omega_{b1}$ [rad/s] | $\omega_{b2}$ [rad/s] | $G$ [$s^{-1}$] | $M$ [s] |
|---|---|---|---|---|---|---|
| 1 | 90 | 90 | 6.0 | 6.0 | - | - |
| 2 | 30 | 30 | 0.2 | 0.2 | - | - |
| 12 | 90 | 30 | 6.0 | 0.2 | 100 | $M_1$ |
| 21 | 30 | 90 | 0.2 | 6.0 | 100 | $M_1$ |

*3. Forcing Functions*

The pursuit tracking tasks performed in the experiment of [10] only used a (multisine) target forcing function signal $f_t$, see Fig. 5; no additional (disturbance) forcing functions were present. The target signal $f_t$ was defined by:

$$f_t(t) = \sum_{n=1}^{N_t} A_t[n] \sin\left(\omega_t[n]t + \phi_t[n]\right) \tag{15}$$

Here, $A_t[n]$, $\omega_t[n]$, and $\phi_t[n]$ represent the amplitude, frequency, and phase shift of the $n^{\text{th}}$ sine wave. The total number of sine waves in the multisine signal is indicated with $N_t$, which in the experiment was equal to 10. The frequencies $\omega_t$ were defined as integer multiples of the fundamental measurement frequency $\omega_m = 2\pi/T_m$ to avoid spectral leakage [8].

While the total measurement time in [10] was $T_m = 90$ s, $f_t$ was chosen to have a fundamental period of $T_m/3$, as this enabled direct comparison three phases in the measurements: a steady-state pre-transition phase, the transition phase, and a steady-state post-transition phase. To ensure steady-state behavior in the first phase of the measurement,

a long run-in time of 20 s was added before the 90-second measurement window. This also enabled participants to achieve steady-state values of rms($\sqrt{|x|}$), a key parameter in the model's adaptive logic, as discussed in Section II.

All values needed to replicate the $f_t$ signal used in [10] are listed in Table 2. Note that two forcing function realizations were used, each with a different set of sinusoid phase shifts $\phi_t$. In [10], the first (Testing) forcing function was used for model fitting, while the second (Validation) signal was used to verify potential overfitting.

**Table 2 Target forcing function settings.**

| | | | Testing | Validation |
|---|---|---|---|---|
| $n$ [-] | $\omega_t$ [rad/s] | $A_t$ [rad] | $\phi_t$ [rad] | $\phi_t$ [rad] |
| 1 | 0.419 | $2.905 \cdot 10^{-2}$ | 2.841 | 3.006 |
| 2 | 1.047 | $1.961 \cdot 10^{-2}$ | 3.319 | 6.037 |
| 3 | 1.885 | $1.020 \cdot 10^{-2}$ | 0.718 | 4.544 |
| 4 | 2.722 | $6.032 \cdot 10^{-3}$ | 0.768 | 2.811 |
| 5 | 3.979 | $3.356 \cdot 10^{-3}$ | 2.925 | 5.917 |
| 6 | 5.655 | $1.983 \cdot 10^{-3}$ | 5.145 | 1.842 |
| 7 | 8.188 | $1.230 \cdot 10^{-3}$ | 2.085 | 3.401 |
| 8 | 10.681 | $9.331 \cdot 10^{-4}$ | 0.383 | 2.998 |
| 9 | 14.032 | $7.541 \cdot 10^{-4}$ | 0.763 | 4.614 |
| 10 | 17.383 | $6.674 \cdot 10^{-4}$ | 3.247 | 2.888 |

*4. Participants and Procedures*

Ten participants, who all had no prior experience with tracking tasks, performed the experiment of [10]. Each participant completed an extended training phase before collecting the data during the experiment phase. Details on how the participants were trained can be found in [10]. All data used in the current paper originate from the experiment phase; the data from the training phase were not used.

In the experiment phase, each participant completed three runs for the steady-state conditions (DYN1 and DYN2) to collect the Testing data-set. Then, for the time-varying conditions (DYN121 and DYN212), for each participant five runs were collected for the Testing data-set and three runs for the Validation data-set. These tracking runs were averaged over for both steady-state (testing data-sets) and time-varying (testing and validating data-sets) conditions. Additionally, as previously mentioned, the experiment data for the time-varying runs consisted of two changes in CE dynamics (DYN121 and DYN212), while in this paper only the first change in the CE dynamics is considered (DYN12 and DYN21).

### B. Data Analysis

This section provides an outline of the steps used to match the adaptive pilot model introduced in Section II to the experiment data of [10], and verify the effects of our proposed model updates (see Section II.C). For this, we follow the four-step analysis as visualized in Fig. 6 and detailed below.

**Step 1: Steady-State Modeling:** The purpose of this step is to obtain a better understanding of the human pursuit tracking model in steady-state conditions, as a starting point for matching it with data from the time-varying conditions from [10]. Due to the different controlled system dynamics than considered in [6], the focus was investigating the variation in model outputs as a function of the $K_p$ and $K_r$ gains, while keeping the neuromuscular system parameters constant, as proposed in [6], $\omega_{nm}$ = 10 rad/s and $\zeta_{nm}$ = 0.707. Furthermore, this analysis was performed for different human pilot time delay ($\tau_e$) settings, varying from 0 to 0.3 s with steps of 0.1 s. This resulted in insights into realistic gain settings for the pursuit tracking task from [10] and how they affect the attained level of tracking performance. Note that in this step the human-in-the-loop experiment data from [10] were not used.

**Step 2: Parameter Estimation:** This step uses the mean steady-state data sets for conditions DYN1 and DYN2. The purpose of this step is to parameterize the modified Hess model for all participants who performed the experiment of [10]. This is accomplished by estimating the human operator gains ($K_p$ and $K_r$) for each participant using a cost

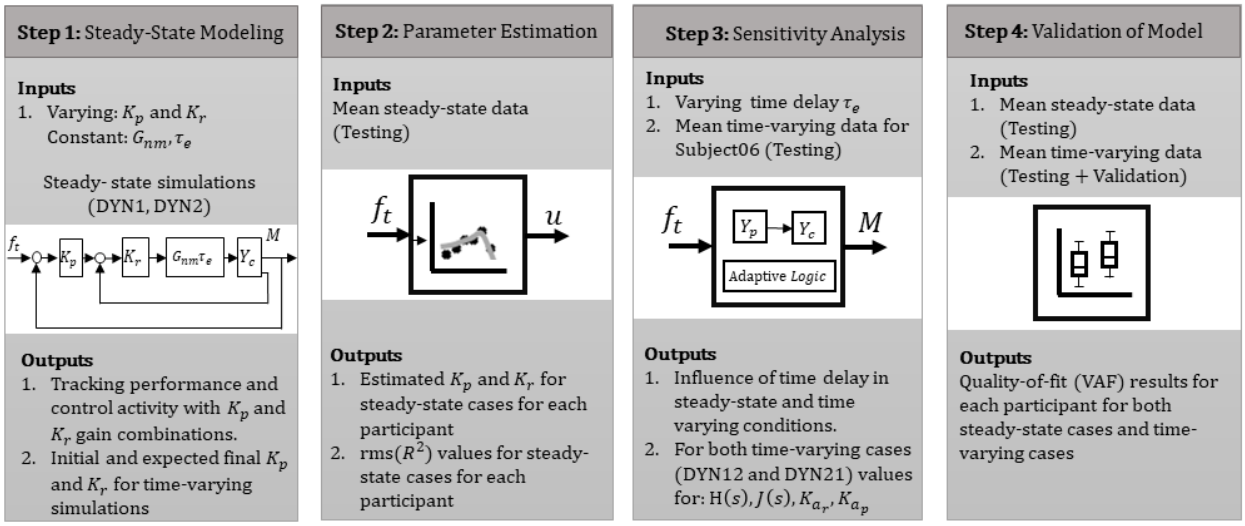


**Fig. 6 Overview of the different steps of analysis followed in this paper.**

function $J$ that fits the model's controller output signal $u_m$ to the measured output signal $u_h$:

$$\arg\min_{\theta} J(\theta) = \frac{1}{K}\sum_{k=1}^{K}(u_h[k] - u_m[k])^2 \tag{16}$$

Here, $K$ is the number of samples in a tracking run and the parameter vector $\theta = [K_r \quad K_p]$. The optimization was implemented in Matlab using the nonlinear solver *fmincon*. To avoid local minima, the optimization was run ten times with different initial conditions on each data set. Overall, the results were consistent across the different optimization runs, suggesting that the real optimum was found. Finally, when suitable gains are found the rms$[R^2(t)]$ value, a key tuning parameter of the model's adaptive logic in Eq. (7), is calculated for each participant and both DYN1 and DYN2.

**Step 3: Sensitivity Analysis:** To investigate the variability in the adaptive pilot model's outputs under changes in its key parameter settings, in this step a sensitivity analysis of the model is performed. This sensitivity analysis was performed with the model tuning for one of the experiment participants from [10] as the baseline. First, the consequences of the added human time delay parameter $\tau_e$ and how with delay some other parts of the model need to be re-tuned was investigated in steady-state (DYN1) and time-varying (DYN12) conditions. Second, the model sensitivity to key model parameters in the Triggering and Adaptation logic – the break frequency of the low-pass filter $H(s)$on the $x$-signal, the adaptation constants $K_{a_r}$ and $K_{a_p}$, and the break frequency of the low-pass filter $J(s)$ on the gain adaptation – was investigated, also focusing on condition DYN12. The quality-of-fit for the adaptive pilot model was quantified using the Variance Accounted For (VAF), a well-known fitting metric [7] that can vary between 1 (perfect model fit) and $-\infty$ (bad model fit), for the region after the CE transition, referred to as the post-transition region. VAF values are calculated for both the pilot control output signal ($u$) and the CE output ($M$) – referred to as VAF$_u$ and VAF$_M$, respectively, and were calculated using the following equation (shown only for VAF$_u$):

$$\mathrm{VAF}_u = 1 - \frac{\sigma^2\,(u_\mathrm{h} - u_\mathrm{m})}{\sigma^2\,(u_\mathrm{h})} \tag{17}$$

**Step 4: Model Validation:** In this final analysis step, we validate the adaptive pilot model for the time-varying conditions DYN12 and DYN21 for all participants in the data set from [10]. For this, the estimated parameters for steady-state pre-transition behavior (DYN1 and DYN2, respectively) are used and the quality of the model for predicting the post-transition behavior adaptation is evaluated using VAF$_u$ and VAF$_M$ (see Eq. (17)). Additionally, the testing and validation data sets from [10] are considered separately for evaluating the model's quality-of-fit, to verify the sensitivity of the model response to the (errors induced by) the forcing function signal. Based on previous studies [7, 10], it is expected that transitions from the single to double integrator (DYN12) are better predicted (higher VAF$_u$ and VAF$_M$) than transitions from double to single integrator (DYN21).

# IV. Results

## A. Step 1: Steady-State Modeling

As explained in Section III.B, the aim of this first analysis is to verify how different combinations of the human operator gain values $K_p$ and $K_r$ affect the output of the pursuit tracking model. As shown in Fig. 7, for both steady-state conditions DYN1 and DYN2 the variation in the root mean square of the error signal (rms($e$)) was used to quantify the level of tracking performance achieved. For both conditions, $K_p$ ranged between 0 and 15 with a step size of 0.01, while $K_r$ ranged between 0 and 0.15 with a step size of 0.01. For the $K_p$ and $K_r$ combinations that result in an unstable closed-loop system no data is shown in Fig. 7, while the 'optimal' gain combination that results in the lowest possible rms($e$) is indicated with a red circle marker. For brevity, only the results for $\tau_e$ = 0.2 s are presented here; equivalent results for all other human time delay settings can be found in [19].

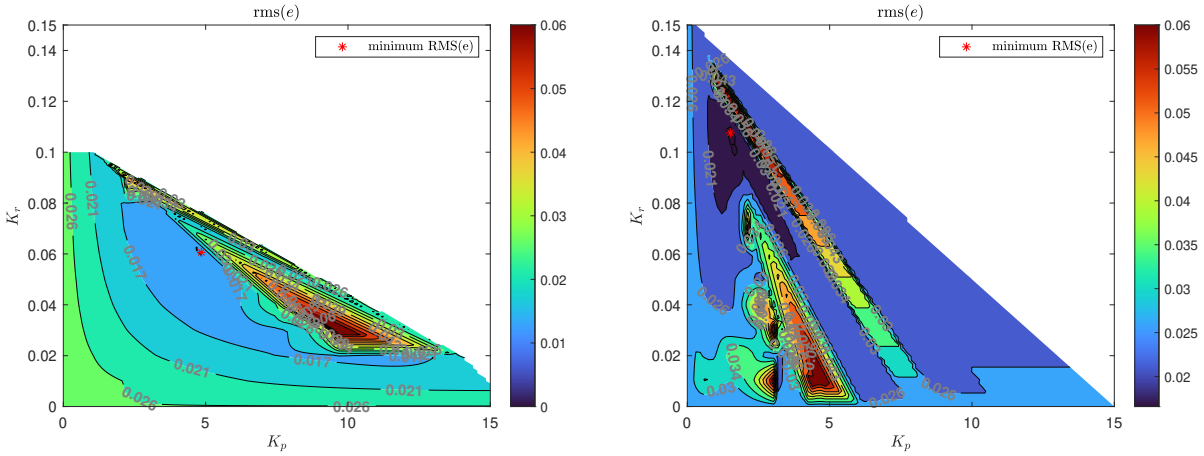


**(a) DYN1** **(b) DYN2**

**Fig. 7 Contour plots showing how different combinations of $K_p$ and $K_r$ values lead to differences in rms($e$) for (a) condition DYN1 (single integrator) and (b) condition DYN2 (double integrator).**

As expected for a closed-loop manual control system [8, 17], Fig. 7 shows that higher gain values lead to better performance until the system becomes unstable. For the DYN1 condition the results of the $K_p$ gain value range from 0 to 15, while $K_r$ gain ranges from 0 to 0.1. The gain values that result in the minimum rms($e$) of 0.013 rad are $K_p$ = 4.82 and $K_r$ = 0.06, which corresponds to a crossover frequency $\omega_c$ = 2.8 rad/s and phase margin $\phi_m$ of 44 deg. For DYN2, feasible $K_p$ and $K_r$ values range from 0 to 15 and 0 to 0.15, respectively. The gain values that result in optimal performance (rms($e$) = 0.016 rad) are $K_p$ = 1.52 and $K_r$ = 0.11, which result in $\omega_c$ = 3.5 rad/s and $\phi_m$ = 5 deg. Fig. 7 thus shows that for a transition from single to double integrator dynamics (DYN12), $K_p$ is expected to decreases while $K_r$ increases after the transition. The opposite is expected for the reverse transition in condition DYN21.

## B. Step 2: Parameter Estimation

Table 3 shows the estimated human operator gain values for DYN1 and DYN2 for all participants in the data set from [10]. Additionally, the table shows the corresponding open-loop stability characteristics and the $\text{VAF}_u$ and $\text{VAF}_M$ quality-of-fit metrics. Overall, the estimated human operator gain values in Table 3 are consistent with the findings of Section IV.A. While the estimated values for the inner-loop gain $K_r$ are quite close to the predicted optimal settings based on Fig. 7 – 0.06 and 0.11 for DYN1 and DYN2, respectively – all participants show much-reduced $K_p$ values. As expected for real human operators, who have to weigh tracking performance against stability and effort [8, 17], this results in less aggressive control behavior characterized by lower $\omega_c$ and increased $\phi_m$. Overall, with crossover frequencies around 1 rad/s for DYN1 and 1.8 for DYN2, the experiment's participants all used a relatively low-gain control strategy, also compared to the $\omega_c$ = 1.50 rad/s Hess [6] tuned his model for. Furthermore, the DYN2 data collected from Subjects 02, 05, and 07 were found to be insufficiently consistent for fitting the model; hence no fitting results are shown for these cases in Table 3.

Overall, the $VAF_u$ and $VAF_M$ data in Table 3 also show that not all participant's data could be modeled at high accuracy. The attained quality-of-fit seems to be dependent on the participants' crossover frequencies: for example, for DYN1 Subject 06 has the highest crossover frequency of 1.58 rad/s and also the highest $VAF_u$ (0.75) value, while Subject 01 has the lowest $\omega_c$ = 0.75 rad/s and by far the worst $VAF_u$ of only 0.38. In our view, this is not necessarily a drawback of the model, but also caused by the (in hindsight) insufficient instruction and too low level of aggressiveness in the experiment of [10]. Given that overall good VAF values were obtained for Subject 06, who also had crossover frequency that matches well with the adaptive model tuning from [6], this participant was selected as the baseline for the sensitivity analysis in Step 3. Furthermore, based on the results of Table 3 the data from Subject 01 were not used for the analysis of the time-varying condition DYN21.

**Table 3 Steady-state fitting results for DYN1 and DYN2.**

| Subject | DYN1 | | | | | | DYN2 | | | | | |
|---|---|---|---|---|---|---|---|---|---|---|---|---|
| | $K_p$ | $K_r$ | $\omega_c$ | $\phi_m$ | $VAF_u$ | $VAF_M$ | $K_p$ | $K_r$ | $\omega_c$ | $\phi_m$ | $VAF_u$ | $VAF_M$ |
| | – | s | rad/s | deg | – | – | – | s | rad/s | deg | – | – |
| 00 | 2.38 | 0.06 | 1.14 | 72.08 | 0.68 | 0.86 | 1.45 | 0.08 | 1.80 | 38.04 | 0.74 | 0.79 |
| 01 | 1.27 | 0.09 | 0.75 | 80.92 | 0.38 | 0.70 | 0.47 | 0.14 | 1.30 | 62.84 | 0.25 | 0.43 |
| 02 | 1.80 | 0.06 | 0.84 | 76.68 | 0.64 | 0.87 | | | | n/a | | |
| 03 | 1.33 | 0.09 | 0.75 | 80.34 | 0.57 | 0.91 | 0.85 | 0.10 | 1.38 | 61.59 | 0.25 | 0.79 |
| 04 | 1.77 | 0.08 | 0.96 | 76.80 | 0.67 | 0.96 | 1.09 | 0.09 | 1.95 | 35.64 | 0.50 | 0.85 |
| 05 | 1.77 | 0.07 | 0.91 | 76.77 | 0.61 | 0.84 | | | | n/a | | |
| 06 | 3.18 | 0.06 | 1.58 | 65.14 | 0.75 | 0.91 | 1.10 | 0.07 | 1.33 | 51.55 | 0.75 | 0.92 |
| 07 | 1.52 | 0.08 | 0.83 | 78.79 | 0.48 | 0.90 | | | | n/a | | |
| 08 | 1.64 | 0.09 | 0.97 | 78.02 | 0.66 | 0.84 | 0.98 | 0.08 | 1.99 | 43.00 | 0.51 | 0.54 |
| 09 | 1.64 | 0.09 | 0.97 | 78.02 | 0.59 | 0.89 | 1.55 | 0.09 | 1.93 | 44.97 | 0.25 | 0.80 |

Due to the fact that a number of the equations in the Triggering and Adaptation blocks of the adaptive pilot model contain scaling terms that depend on the baseline pre-transition level of performance, see Section II, the between-participant differences in task performance and crossover frequency observed from Table 3 will also affect the adaptive part of the model. To investigate this, Fig. 8 plots two of those parameters, rms($x$) and rms($R^2$), as a function of each other, while the marker color map shows the corresponding tracking error magnitude rms($e$). Each marker is labeled with the corresponding participant number. Fig. 8 shows that indeed the participants with the lowest crossover frequency (Subjects 01 and 03, 0.75 rad/s) show the highest rms($e$) of 0.0192 and 0.0193 rad, respectively. Subject 06, with the highest crossover frequency of 1.58 rad/s, also shows the lowest error value of rms($e$) = 0.0154 rad. Fig. 8 further shows that for our experiment data rms($x$), rms($R^2$), and rms($e$) are all correlated. For example, we see that the magnitude of the $x$ signal varies across the participants and that rms($x$) is around six times smaller for Subject 01 than for Subject 06. Consequently, the $X_n$ signal as defined in Eq. (7) also varies considerably in magnitude per subject. As the magnitude of $X_n$ directly scales the update of the adaptive pilot model gains $K_p$ and $K_r$, the values of the adaptation constants $K_{a_r}$ and $K_{a_p}$ will need to be participant-based to avoid under- or overreacting of the models parameter adjustments.

### C. Step 3: Sensitivity Analysis

*1. Effects of human operator time delay*

A sensitivity analysis was performed to analyse the effects of the introduced human time delay $\tau_e$ on the adaptive model's response, for both a steady-state (DYN1) and time-varying (DYN12) condition. Please note that for this analysis the $K_p$ and $K_r$ settings for Subject 06 (see Table 3) are used. Furthermore, the settings of the low-pass filter $H(s)$ on the $x$ signal were kept constant and equivalent to those used by Hess [6], i.e., $\omega_{lp}$ = 1.5 rad/s and $\zeta$ = 1. Finally, the delay $\tau_e$ was varied over four settings: 0, 0.1, 0.2, and 0.3 s. It should be noted that while in reality a change in human delay would generally be accompanied by a change in human operator gains (see, e.g., [8, 17, 20], here the $K_p$ and $K_r$ gains were kept constant for all compared $\tau_e$ values. While this is a limitation of the analysis, it is the best method to show the influence of the time delay in the model.

The results of the analysis on the steady-state DYN1 data are shown in Fig. 9. As the CE dynamics do not change in this condition, the models Triggering should not be activated. Fig. 9a shows the influence of the human pilot delay $\tau_e$ on

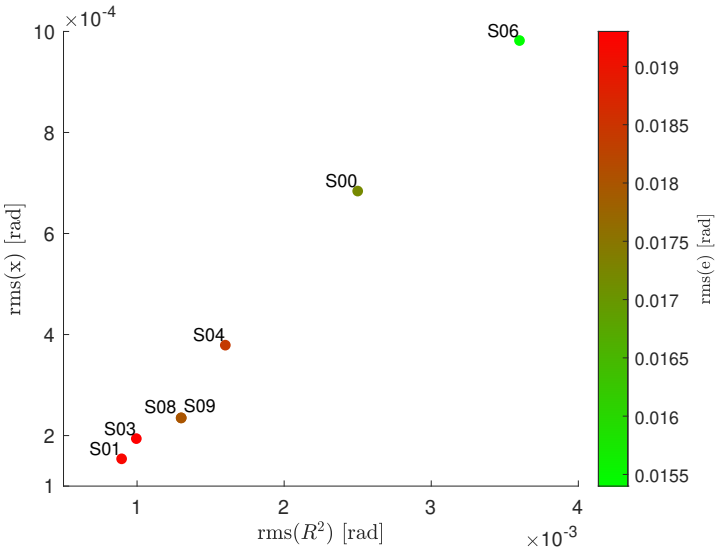


**Fig. 8 Correlation plot of rms$(x)$, rms$(R^2)$, and rms$(e)$ for all experiment participants. Please note that the data for Subjects 08 and 09 overlap.**

the $x$ signal. The top graph shows the $x$ signal before it is filtered by $H(s)$, while the bottom graph shows the filtered $x$ signal. For $x$ it can be observed that increased delay results in an increase of the magnitude in the $x$ signal, as expected: a larger delay introduces larger tracking errors, see also Fig. 9b. Thus, a larger $\tau_e$ means that the Adaptation would induce stronger changes in $K_r$ and $K_p$ due to the larger magnitude of $x$ and $X_n$. Therefore, the introduced adaptation constants, $K_{a_r}$ and $K_{a_p}$ (see Section IV.C.3), are needed to counter this potential overreaction.

To analyze the effect on the Triggering logic, Fig. 9c explicitly shows the model's triggering criterion as defined in Eq. (5) in normalized form, i.e., $\sqrt{|x|}/\text{rms}\sqrt{|x|} > 3$. This means that any signal peaks that exceed the trigger threshold of 3, indicated with a horizontal green line in Fig. 9c, will result in Triggering activation. Any Triggering activation is shown in Fig. 9d, which plots the $K_{trigger}$ signal. Matching Fig. 9a, the top graphs show the results when the $x$ signal is not filtered by $H(s)$, while the bottom graphs show results obtained with the filtered $x$ signal. From Fig. 9c and 9d it can be observed that the effect of $\tau_e$ on the Triggering mechanism is found to be small. However, this is at least partly due to the applied filter $H(s)$, as the filter smooths out instantaneous peaks in $x(t)$, which would otherwise cause false positives as seen in Fig. 9d (top).

Due to the time delay effects shown in Fig. 9, having a time delay in the model will also affect the model's Triggering and Adaptation mechanisms. Here, we show this for condition DYN12, for which the CE dynamics transition from an effective single-integrator dynamics to an approximate double-integrator dynamics at $t$ = 30 s, see Fig. 10. From this figure, it can be observed that an increase in $\tau_e$ results in an increase in magnitude of the post-transition error peak in the model, see Fig. 10a. The tested delay values of 0, 0.1, 0.2, and 0.3 result in peaks in $x(t)$ that are 8%, 16%, 22%, and 27% higher than the triggering limit, respectively, and longer duration of the $K_{trigger} = 1$ spike shown in Fig. 10b. As discussed in Section IV.B, increased magnitude of $x(t)$ results in a larger gain adjustments through the Adaptation mechanism that may need to be corrected for with $K_{a_p}$ and $K_{a_r}$.

Finally, for the experiment data of [10] that we consider in this paper, the human operator delay values for all participants were measured to be approximately 0.2 s for all participants and test conditions. While a limitation, as in reality time delays are known to vary between different operators, a $\tau_e$ of 0.2 s was implemented in the model for all participants and is used in the remainder of the paper. Please note that this constant delay across participants is consistent with the 'universal' neuromuscular dynamics setting also proposed in [6].

*2. Effects of Triggering logic filter $H(s)$*

The second focus point for our sensitivity analysis is the low-pass filter $H(s)$ that is applied to the $x$ signal to smooth out brief and instantaneous peaks (extreme values) that would otherwise cause many false positives in the Triggering and Adaptation mechanisms when not in fact required [6], see also Fig. 9. As explained by Hess [6], human operators

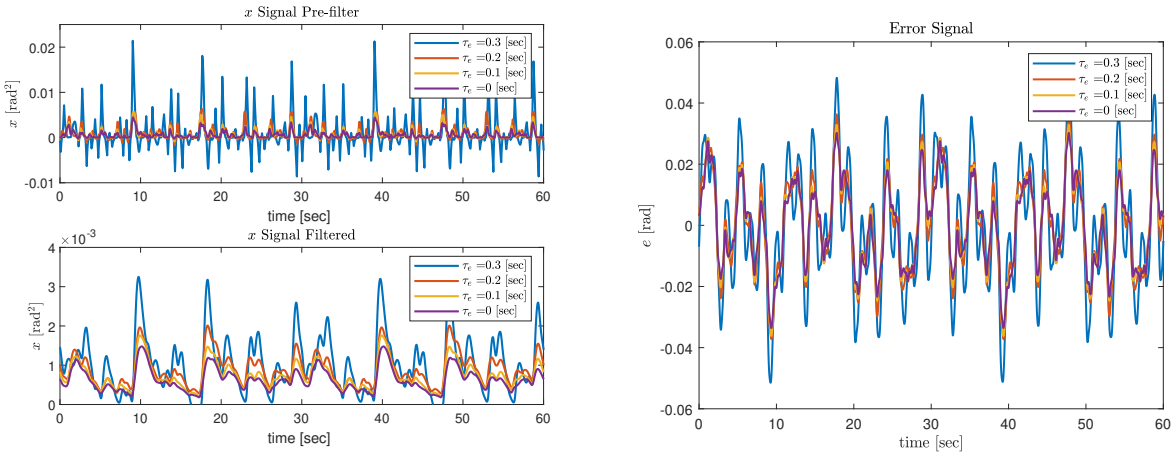


**(a) $x$-signal**




**(b) Error signal**

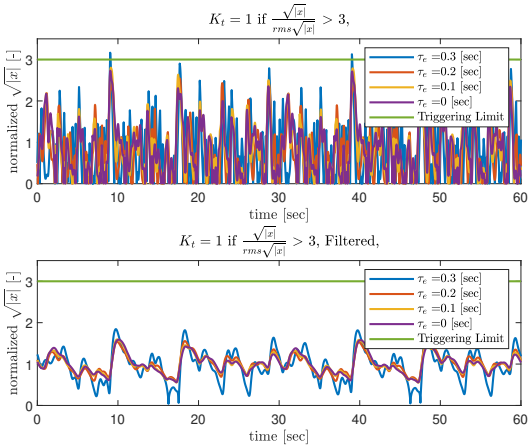


**(c) Triggering logic**

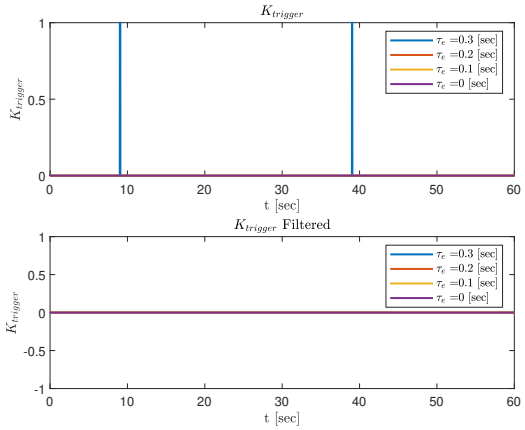


**(d) Trigger signal**

**Fig. 9 The effect of increasing the time-delay $\tau_e$ in a DYN1 steady-state system on (a) the $x$-signal, where the top graph shows the unfiltered signal and the bottom graph the filtered signal, (b) the tracking error signal $e$, (c) the Triggering logic, and (d) the time during which the Triggering logic is activated ($K_{trigger}$ signal), for both the unfiltered (top), and filtered (bottom) $x$-signals.**

will not directly change their control strategy for any brief off-nominal control error that occurs. As defined in Eq. (4), a second-order low-pass filter with $\omega_{lp}$ = 1.5 rad/s and $\zeta$ = 1 is applied on the $x$ signal to model this effect. Here, we investigate the influence of the choice of $\omega_{lp}$ by varying the bandwidth of $H(s)$ across four different settings: 1, 2, 3, and 4 rad/s. The results of this analysis, again performed with the gain settings for Subject 06 and the time-varying condition DYN12, are shown in Fig. 11.

Fig. 11 shows that reducing the low-pass filter bandwidth induces lag in the $x$ signal and hence also the model's Triggering. Fig. 11b shows that trigger activation at 3.8, 2.2, 2 and 1.9 s after the CE transition for $\omega_{lp}$ = 1, 2, 3, 4 rad/s, respectively. A higher $\omega_{lp}$ reduces lag and also attenuates the magnitude of $x(t)$ to a lesser degree, see Fig. 11a, which allows for more of the peaks to pass $H(s)$, thus causing the triggering to take place earlier. A too low $\omega_{lp}$ in $H(s)$ can thus result in the adaptive logic being activated later than real human operators would do, or even cause Triggering to not be activated at all. The results in Fig. 11 show that for the specific participant considered here (Subject 06), who has a similar crossover frequency $\omega_c$ as used for the original Hess model's tuning, the $\omega_{lp}$ = 1.5 rad/s proposed in [6] would be a suitable value to use. However, as for participants with a higher or lower $\omega_c$ the frequency content of $x(t)$ will be different, using the same $\omega_{lp}$ will likely result in a Triggering mechanism that is too sensitive or too

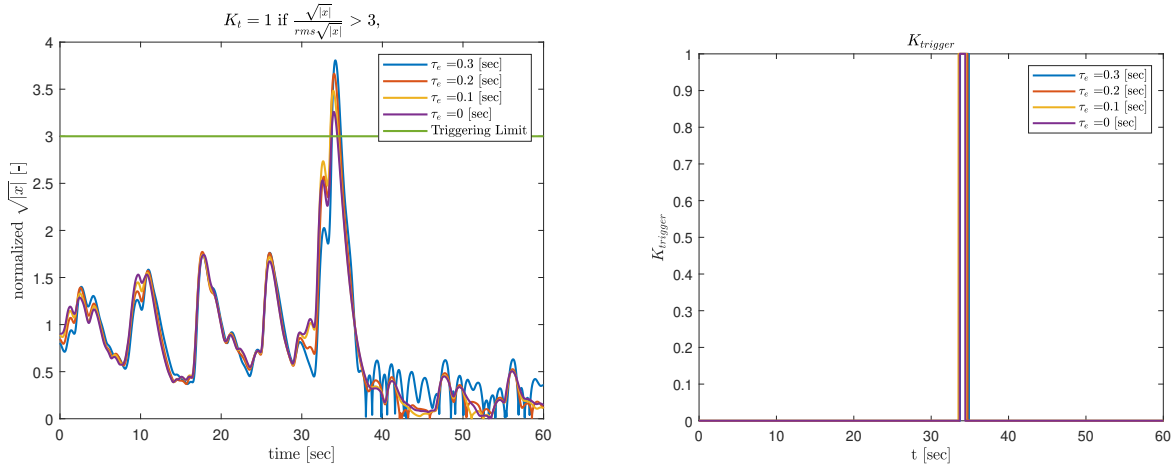


**(a) Triggering logic** **(b) Trigger signal**

**Fig. 10 The effect of increasing the time delay $\tau_e$ for the time-varying DYN12 scenario on (a) the Triggering logic, and (b) the moments at which the Trigger logic is activated ($K_{trigger}$ signal), where $H(s)$ is active.**

conservative, respectively. This means that to retain the same sensitivity, either the value of $\omega_{lp}$ or the lower Triggering limit (horizontal green line in Fig. 11b) would need to be adjusted.

*3. Effects of Adaptation constants $K_{a_r}$ and $K_{a_p}$*

The adaptation constants, $K_{a_r}$ and $K_{a_p}$, scale the change of $K_r$ and $K_p$ as described in Eq. (6) and (9), respectively. While not explicitly included in the original model definition in [6], the adaptive model presented by Hess used $K_{a_r}$ = 1 and $K_{a_p}$ = 0.35 for the modeled CE transition also shown in Fig. 3 and 4. As the specific $K_r$ and $K_p$ gain values that will be used by human operators can vary widely for different CE dynamics, displays, and forcing function settings, also $K_{a_r}$ and $K_{a_p}$ will need to be adjusted between different modeled tasks. For example, as can be verified from Table 3, for Subject 06 $K_p$ = 3.18 and $K_r$ = 0.06 for the pre-transition DYN1 dynamics, while for DYN2 $K_p$ = 1.10, $K_r$ = 0.07. This shows that for the DYN12 CE transition investigated here (and in [10]), we expect $K_r$ to increase while $K_p$ decreases. Also, as the difference in magnitude between both gains is much larger for our current case than considered in [6], also $K_{a_r}$ and $K_{a_p}$ will need to differ much more in magnitude for the DYN12 CE transition than for Hess's CE transition [6]. Table 4 shows the VAF values for the model output $M$ and control output $u$ across a feasible range of $K_{a_r}$ and $K_{a_p}$ values for our considered data set. As $K_{a_r}$ = 0.0055 and $K_{a_p}$ = -150 lead to the highest VAF$_u$ and VAF$_M$, these values were chosen to be used in the adaptive model. In order to show the influence of $K_{a_r}$ and $K_{a_p}$ on the adaptation of $K_r$

**Table 4 VAF results for varying the adaptation constants $K_{a_r}$ and $K_{a_p}$.**

| $K_{a_r}$ | $K_{a_p}$ = -150 | | $K_{a_p}$ = -200 | | $K_{a_p}$ = -250 | |
|---|---|---|---|---|---|---|
| | VAF$_M$ | VAF$_u$ | VAF$_M$ | VAF$_u$ | VAF$_M$ | VAF$_u$ |
| 0.0035 | 0.39 | -3.25 | 0.87 | 0.64 | 0.85 | 0.67 |
| 0.0040 | 0.65 | -1.02 | 0.90 | 0.79 | 0.73 | 0.46 |
| 0.0045 | 0.83 | 0.31 | **0.89** | **0.76** | 0.41 | 0.21 |
| 0.0050 | 0.89 | 0.73 | 0.72 | 0.47 | 0.12 | 0.09 |
| 0.0055 | **0.91** | **0.81** | 0.52 | 0.28 | 0.00 | 0.00 |
| 0.0060 | 0.89 | 0.78 | 0.19 | 0.11 | 0.00 | 0.00 |

and $K_p$, two combinations of the adaptation gains were selected from Table 4 as an example, see values highlighted in bold. Fig. 12 shows how the $K_r$ (top graph) and $K_p$ (bottom graph) gains adapt for these two cases. Both graphs show that with appropriate $K_{a_r}$ and $K_{a_p}$ the model is able to induce the required increase in $K_r$ and decrease in $K_p$ that is needed for the DYN12 CE transition. Furthermore, Fig. 12 shows that the magnitude of the post-transition gain values is directly controlled with $K_{a_r}$ and $K_{a_p}$: the increase in $K_r$ with respect to its pre-transition value scales directly

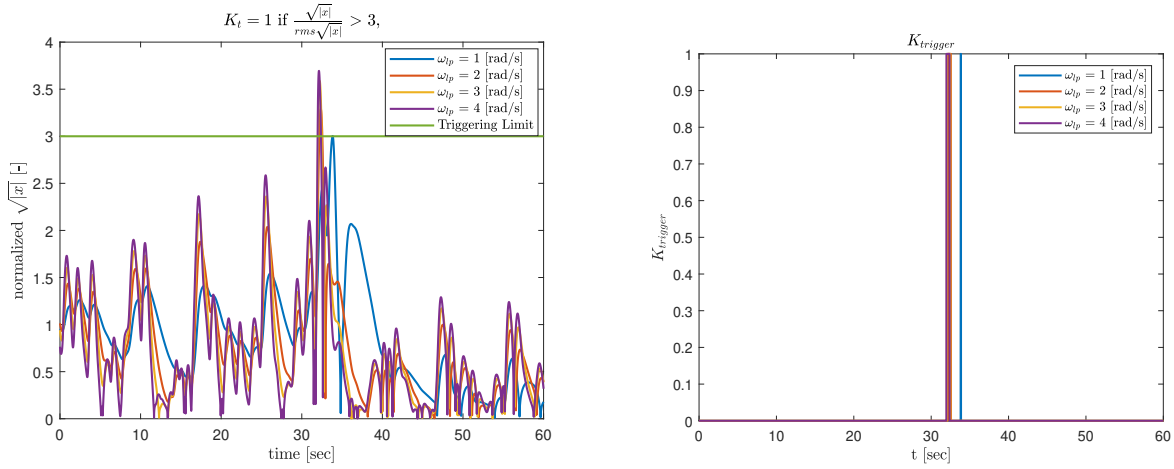


**(a) Triggering logic** **(b) Trigger signal**

**Fig. 11 The effect of varying the $H(s)$ filter's break frequency $\omega_{lp}$ in condition DYN12 on (a) the Triggering logic, and (b) the triggering signal $K_{trigger}(t)$.**

with $K_{a_r}$, while the difference in the $K_p$ reduction between both cases is smaller than reflected by $K_{a_p}$ only, as $\Delta K_p$ is proportional to $K_{a_r} K_{a_p}$, see Eq. (9). This makes the adaptation gains crucial (and very sensitive) parameters to adapt for making the model proposed by [6] match with different CE transitions and experimental data sets.

Finally, Fig. 12 shows clear spikes in the gain values that occur due to the scaling with $X_n(t)$ (see Eq. (6) and Fig. 2). The prominence of such spikes on the $K_r$ and $K_p$ traces are also strongly affected by the settings of the low-pass filter $J(s)$ that is applied to the change in gains, see also Section IV.C.4.

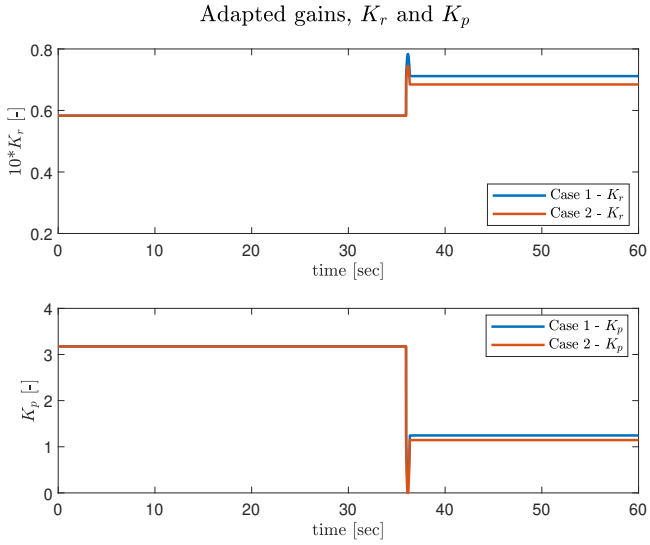


**Fig. 12 Gain adaptations with varying adaptive constants: Case 1 has $K_{a_r} = 0.0055$, $K_{a_p} = -150$, while Case 2 has $K_{a_r} = 0.0045$, $K_{a_p} = -200$.**

*4. Effects of Adaptation gain filter $J(s)$*

As human operators are unlikely to show instantaneous gain adjustments after a CE transition, Hess [6] included a second-order low-pass filter $J(s)$ with $\omega_{lp} = 1$ rad/s and $\zeta_{lp} = 1$ on the parameter adaptation, see Eq. (8). With these settings, a step-like gain transition is smoothed to take over 5 s. To verify how the $J(s)$ filter settings affect the fit

to experimental data, we performed a sensitivity analysis to investigate the effects of $\omega_{lp}$ on the model's Adaptation. Settings for $\omega_{lp}$ ranging from 1 to 10 rad/s, and including $\omega_{lp} = \infty$ rad/s (no filtering, NF), were tested. The $J(s)$ filter affects the model's output directly after triggering occurs, as indicated with the shaded gray 'transition region' in Fig. 13. In the transition region, the model's tracking output $M$ for low values of $\omega_{lp}$ shows larger oscillations and slower stabilization than for higher $\omega_{lp}$, as expected.

Fig. 14 shows the corresponding effects of $J(s)$ on the model's $K_p$ and $K_r$ gain adaptation. For the case without filter (NF), Fig. 14 shows that, as expected, the change in gains is instantaneous, whereas for the case with the lowest filter bandwidth ($\omega_{lp}$ = 1 rad/s) the gain adjustment takes more than 5 s. This difference directly explains the variation in tracking performance with $\omega_{lp}$ seen in Fig. 13a. Additionally, for $\omega_{lp} > 5$ rad/s Fig. 14 shows a clear dip directly when the $K_p$ gain transitions. This dip results from the transient of the $X_n$ signal during the time the Triggering is activated, see Fig. 2. When $\omega_{lp} < 5$ rad/s, this key behavior of the model's Adaptation mechanism is filtered out by $J(s)$, resulting in a fully smooth gain transition. An optimal value for $\omega_{lp}$ was selected based on the best quality-of-fit compared to our measured data for Subject 06 in the transition region. As is also clear from Fig. 13a, the quality of model fit in the transition region was found to be relatively poor, as the measured human adaptation occurred quicker than that of the model's adaptive scheme. Still, VAF values for the control output ($u$) and model output ($M$) improved with increasing $\omega_{lp}$ and were best for the case without a filter (NF): $\text{VAF}_u = -21.2$ and $\text{VAF}_M = -2.8$, compared to $\text{VAF}_u = -71.8$ and $\text{VAF}_M = -11.0$ for the $\omega_{lp} = 1$ rad/s proposed in [6]. Thus, the best fit to our data is obtained for a step-like adaptation of the human operator gains, which is consistent with a previous study by Zaal [7], who also found near-instantaneous changes in human operator control behavior.

### D. Step 4: Model Validation Results

In Section IV.C a model sensitivity analysis was performed based on the experiment data from a single participant (Subject 06). This section adds model validation for all participants in the experiment data set from [10], focusing on the time-varying conditions DYN12 and DYN21. It should be noted that model fitting results for the steady-state conditions (DYN1 and DYN2), which are used as individual participants' reference parameters in this analysis, can be found in Section IV.B.

#### *1. Condition DYN12*

In condition DYN12 the CE transitions from approximate single-integrator to dynamics that approximate a double integrator. With the estimated value for the $H(s)$ filter's break frequency ($\omega_{lp}$ = 1.5 rad/s) based on the data from Subject 06 (see Section IV.C.2), it was found that the Triggering mechanism was only activated for Subject 06's data. To increase the Triggering mechanism's sensitivity to ensure activation for more of the participants, the bandwidth of the filter $H(s)$ was increased to $\omega_{lp}$ = 3 rad/s for all participants. As can be seen from Fig. 15, which shows the normalized $\sqrt{|x|}$ signal for Subject 00 as an example, increasing the bandwidth of $H(s)$ results in a larger magnitude of the $x$-signal and successful Triggering activation (see blue data).

As a result of increasing the bandwidth of $H(s)$, as also discussed in Section IV.C.2, the magnitude of the gain adaptation will also increase, due the increased magnitude of the $x$ and $X_n$ signals. To ensure that the model's post-transition $K_r$ and $K_p$ values still match with the steady-state values expected for DYN2, the gain adaptation constants $K_{a_r}$ and $K_{a_p}$ also need to be adjusted (and decreased) for all participants. Even with such parameter adjustments, with the pre-transition gain values identified for Subject 01 and 03 it was found impossible to activate the Triggering mechanism for these participants. Hence, no data are shown for these participants in Table 5, which summarizes the model's parameters for all participants as used for the validation tests. Table 5 lists the initial $K_p$ and $K_r$ gain values of the pre-transition phase (determined in Section IV.B) and their corresponding open-loop stability characteristics.

Table 6 further shows the final adapted gains of the post-transition phase results for both the testing and validation data sets from [10]. Both data sets were used to verify if time-varying modeling artefacts occur due to specific forcing function patterns in the transition region and to detect potential overfitting of the testing data. When no adapted gain values are listed in Table 6, the Triggering mechanism did not activate and thus no adaptation of the modeled human operator's gains occurred. Additionally, the open-loop stability characteristics are provided, which still vary due to the CE transition even if the adaptive operator model is not Triggered.

Comparing Table 5 and Table 6 shows that when the adaptation is triggered for Subjects 00, 04, and 06, the inner-loop gain $K_r$ increases as expected, as the CE change requires the generation of added lead in the feedback control [8, 10]. For Subjects 08 and 09, on the other hand, only very slight adjustments to $K_r$ and $K_p$ were found compared to the

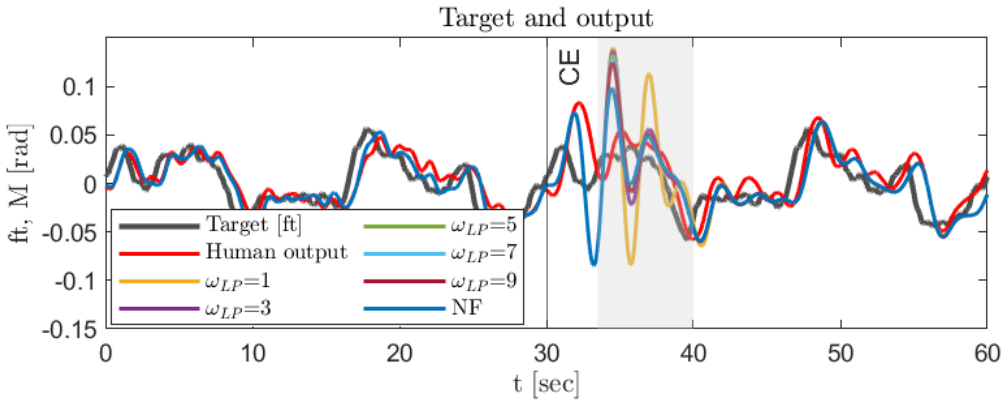


**(a) Tracking signals**

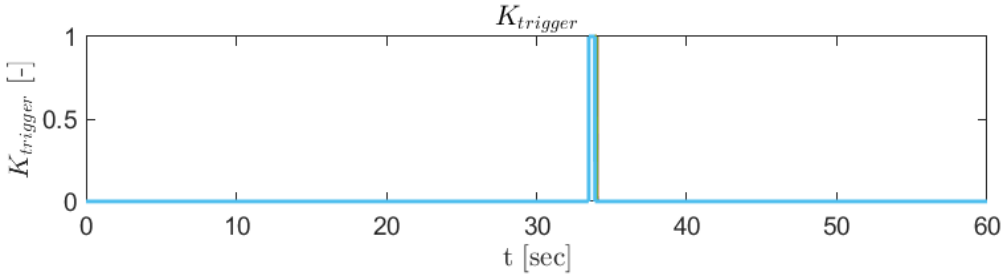


**(b) Trigger signal**

**Fig. 13 Effects of the $J(s)$ filter break frequency on the adaptive model's output: (a) tracking performance and (b) Triggering activation.**

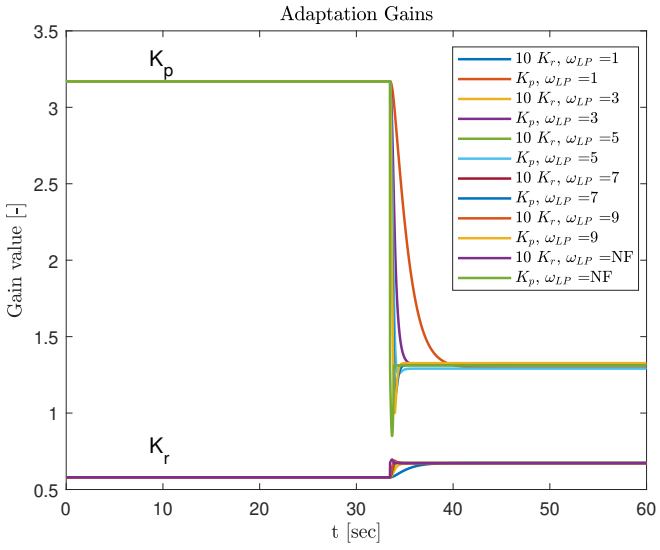


**Fig. 14 Gain adaptations with varying the parameter $\omega_{lp}$ of the filter $J(s)$.**

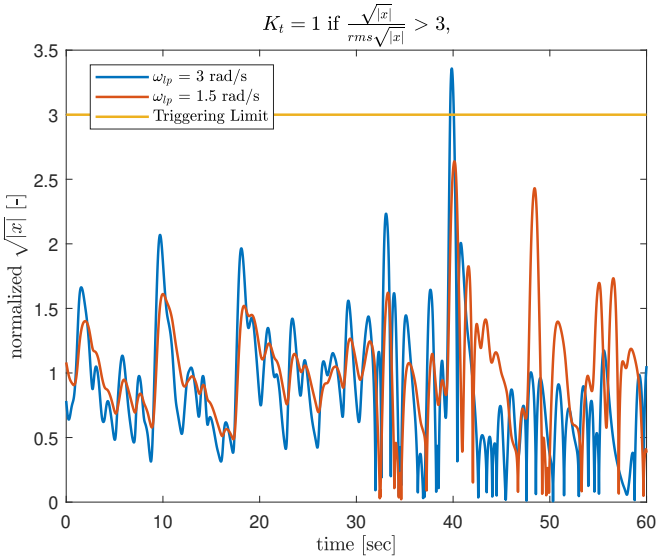


**Fig. 15 Effect of increasing $\omega_{lp}$ of the $H(s)$ filter from 1.5 rad/s to 3 rad/s on the Triggering mechanism for Subject 00.**

pre-transition DYN1 settings from Table 5. This can be explained by the fact that these participants already had a high $K_r$ gain in the pre-transition phase (0.016 points above average). Hence, their control strategy was already effective for DYN2, which resulted in only momentary Triggering activation and negligible Adaptation.

As can be seen from Table 6, the Triggering mechanism did not activate for the validation data for Subjects 04, 08, and 09, while the model was triggered for the testing data. As the only difference between the testing and validation data are the used phases for the forcing function (see Table 2), this suggests a potentially strong interaction of the model's Triggering and Adaptation logic with specific temporal features of the forcing function signal around the moment of the CE change. To analyze this effect, a Monte Carlo analysis was conducted where the time at which the CE dynamics transitioned, here referred to as $M_1$, was varied for both the testing and validation forcing functions from 10 to 50 seconds, for a total of 1,000 different $M_1$ settings, see the green shaded area in Fig. 16. The bottom graphs show the time of first Triggering activation plotted on the same time axis as the forcing function signals, with Fig. 16a showing the results for the testing forcing function and Fig. 16b showing the same results for the validation forcing function. The patterns in the histograms show that Triggering mostly occurred when the gradient of the forcing function was relatively large. This is particularly evident for the validation data in Fig. 16b, as the validation forcing function signal also has more standout instances of large gradients. Overall, these results thus confirm the crucial sensitivity of the model's adaptive mechanism to specific features in, and hence the design of, the forcing function signal.

Overall, the Triggering mechanism was activated for 53% and 74% of the tested $M_1$ settings for the testing and validation cases, respectively. When the CE dynamics transition at a moment when the forcing function is constant or has a shallow gradient, the tracking error (and hence the $x$ signal) may not directly increase in magnitude to activate the Trigger. As the Triggering is activated based on the trigger limit ($3\text{rms}(\sqrt{|x|})$), a reference value of that also slowly increases after a CE transition, this can result in a missed trigger. An example of such a case is shown in Fig. 17, where Fig. 17a shows the tracking performance of the model and Fig. 17b shows the $\sqrt{|x|}$ signal and the trigger limit $3\text{rms}\sqrt{|x|}$. In this example, the CE dynamics transitioned at 30 s and the $\sqrt{|x|}$ signal does show a clear spike as a result, see Fig. 17b, however, the spike does not exceed the trigger limit. At around 50 s, a second large spike is evident in $\sqrt{|x|}$, but by then the recursively calculated trigger limit value has increased and again the Triggering is not activated. Overall, this indicates that the Triggering mechanism implemented in the adaptive model from [6] is prone to the strong interaction between the implemented Triggering mechanism and the occurrence of large peaks and gradients in the forcing function signal.

**Table 5 Model parameter settings for model validation for time-varying condition DYN12.**

| Subject | DYN1 Initial gain values | | DYN1 Open-loop characteristics | | Key Model Parameters | | | |
|---|---|---|---|---|---|---|---|---|
| | $K_p$ [-] | $K_r$ [-] | $\omega_c$ [rad/s] | $\Phi_m$ [deg] | $H(s)$ $\omega_{lp}$ [rad/s] | $J(s)$ $\omega_{lp}$ [rad/s] | $K_{a_p}$ [-] | $K_{a_r}$ [-] |
| 00 | 2.379 | 0.058 | 1.138 | 72.076 | 3 | $\infty$ | -40 | 0.17 |
| 01 | 1.266 | 0.095 | 0.753 | 80.921 | - | - | - | - |
| 03 | 1.325 | 0.085 | 0.753 | 80.338 | - | - | - | - |
| 04 | 1.773 | 0.067 | 0.906 | 76.768 | 3 | $\infty$ | -150 | 0.038 |
| 06 | 3.175 | 0.058 | 1.577 | 65.137 | 3 | $\infty$ | -150 | 0.0055 |
| 08 | 1.642 | 0.091 | 0.972 | 78.024 | 3 | $\infty$ | -10 | 0.05 |
| 09 | 1.642 | 0.091 | 0.972 | 78.024 | 3 | $\infty$ | -5 | 0.03 |

**Table 6 Gain adaptation validation results for condition DYN12 for both testing and validation data.**

| Subject | Testing data-sets | | | | Validation data-sets | | | |
|---|---|---|---|---|---|---|---|---|
| | DYN2 Adapted gain values | | DYN2 Open-loop characteristics | | DYN2 Adapted gain values | | DYN2 Open-loop characteristics | |
| | $K_p$ [-] | $K_r$ [-] | $\omega_c$ [rad/s] | $\Phi_m$ [deg] | $K_p$ [-] | $K_r$ [-] | $\omega_c$ [rad/s] | $\Phi_m$ [deg] |
| 00 | 1.465 | 0.080 | 1.529 | 51.949 | 1.472 | 0.080 | 1.537 | 51.585 |
| 01 | - | - | 1.300 | 62.839 | - | - | 1.300 | 62.840 |
| 03 | - | - | 1.358 | 58.380 | - | - | 1.358 | 58.380 |
| 04 | 1.263 | 0.070 | 1.235 | 55.794 | - | - | 1.840 | 34.086 |
| 06 | 1.244 | 0.071 | 1.218 | 56.796 | 1.275 | 0.071 | 1.252 | 55.681 |
| 08 | 1.660 | 0.088 | 1.881 | 45.558 | - | - | 1.991 | 43.000 |
| 09 | 1.653 | 0.089 | 1.877 | 46.392 | - | - | 1.933 | 44.974 |



*2. Condition DYN21*

For the time-varying condition DYN21 the opposite CE dynamics transition occurs compared to DYN12, i.e., from an approximate double integrator to an approximate single integrator, see Table 1. For DYN21, it was found that the adaptive logic was not triggered by the CE change for any of the participants. This is consistent with earlier results from [10] and indicates that while the CE dynamics do change the pre-transition human operator gain settings still provide a satisfactory level of tracking performance, as post-transition CE dynamics in fact are more easily controlled and require less compensation. Without loss of tracking performance after the CE transition, also the model's $x$-signal will not increase in magnitude, as shown in Fig. 18 for an example single participant. Equivalent results were obtained for all other participants in the validation data set. In Fig. 18 the CE dynamics transition at 30 s to the single integrator and the magnitude of the $\sqrt{|x|}$ signal is even seen to decrease even without human operator gain adjustments after the transition.

Fig. 19 shows $\text{VAF}_u$ and $\text{VAF}_M$ quality-of-fit results for both the pre- and post-transition phases in condition DYN21, i.e., the 0-30 and 40-60 s intervals of the 60-second tracking runs. As no Triggering and Adaptation was activated for any of the participants, Fig. 19 shows the results for a non-adaptive model, for which the $K_r$ and $K_p$ gains are the same before and after the CE transition. The $\text{VAF}_u$ data show that the quality-of-fit for the control activity $u$ decreases only slightly (by 0.04 points) in the post-transition range for both the testing and validation data sets, while $\text{VAF}_M$ values are consistently higher. The increase in $\text{VAF}_M$ is consistent with the steady-state fits for DYN1 and DYN2, see Section IV.B, where DYN1 VAF values were also consistently higher than those for DYN2. These high post-transition VAF values indicate that, even without adapting $K_r$ and $K_p$ to the CE change, the model still fits the post-transition single-integrator CE data at high accuracy. Overall, the results presented here for DYN21 indicate that the adaptive logic of the model proposed by Hess [6] – also having been designed to investigate transitions from CE dynamics that are easier to control to more challenging CE dynamics – can not predict the behavioral adaptation that real human operators for transitions that do not directly result in degraded tracking performance.

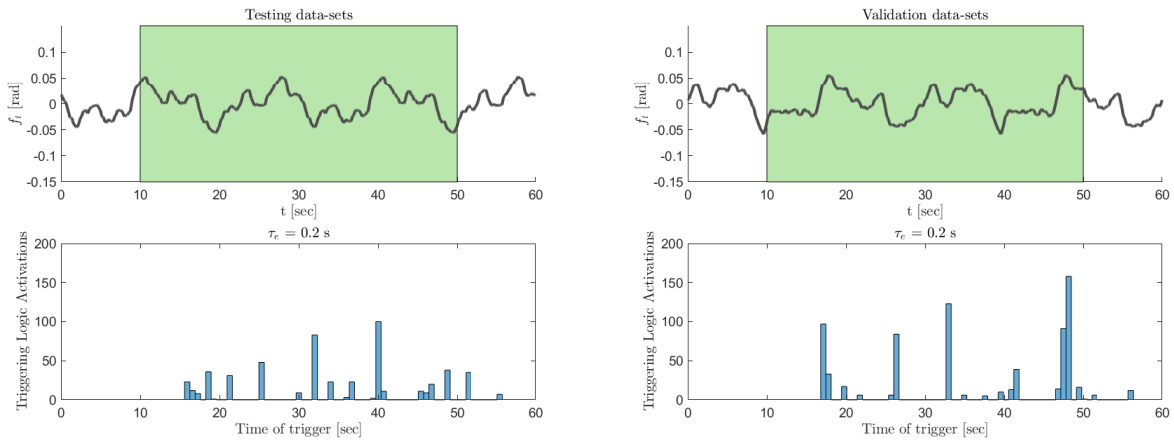


**(a) Testing data** **(b) Validation data**

**Fig. 16 Analysis of Triggering activation for varying CE transition time $M_1$ for (a) the testing forcing function and (b) the validation forcing function.**

## V. Discussion

The work described in this paper aimed at improving our understanding of adaptive human manual control behavior, with an analysis of the adaptive pilot model proposed by Hess [6, 12, 13] and by matching it with previously collected experiment data for a pursuit tracking task with induced time-varying changes in the CE [10]. To investigate the key characteristics of Hess' proposed modeling framework and verify the need for adjustments, we found it necessary to accurately describe our experiment data, and performed an analysis in four steps, as described in Section III, from which the main findings and implications will be discussed in this section.

In Step 1 of our analysis, we investigated the model's inner- and outer-loop gains setting that would be needed when controlling our pre-transition (DYN1, an approximate single integrator) and our post-transition (DYN2, an approximate double integrator) CE dynamics in steady-state. Based on an analysis of the model's tracking performance as a function of its gain settings, we found that for a transition from DYN1 to DYN2 human operators would need to decrease $K_p$ and increase $K_r$. This is consistent with what would be expected when comparing human control dynamics with single- and double integrator CE dynamics: the latter requires more lead (increased $K_r$) and reduced low-frequency response magnitude (reduced $K_p$) [8, 17]. Due to the choice for solely failed systems with reduced responsiveness (lower CE gain), the published adaptive model logic as described in [6] can only model *increases* in the human operator control gains. Hence, this analysis showed that for matching the experiment data of [10], and all other time-varying scenarios where not only post-transition human operator gain increases would be expected, the adaptive logic of the model needs to be adapted.

In Step 2, we fitted the adaptive pilot model to the (steady-state) experiment data collected from 10 participants in [10]. Overall, the data for condition DYN1 could be modeled at high accuracy for all participants, while it proved impossible to achieve a sufficient fit for the DYN2 data for three participants (Subject 02, 05, and 07). Furthermore, the $\text{VAF}_u$ values we used for assessing the model's quality-of-fit were 0.63 and 0.5 on average for conditions DYN1 and DYN2, respectively. In [10], the same experiment data could be modelled with a different human control model at $\text{VAF}_u$ = 0.64 and 0.75 for DYN1 and DYN2, respectively. Also in earlier experiments it was generally found that higher VAF values were obtained for DYN2 data than for DYN1 [7, 15]. These different outcomes for our current work may be explained by the fact that for the model from [6], key human operator's limitation parameters – i.e., the neuromuscular dynamics, which we also extended to the human time delay $\tau_e$ – fixed at 'one-size-fits-all' values. While previous research suggests that these parameters may be considered invariable for the CE transitions (between DYN1 and DYN2) considered in this paper [7, 21], an essential step to improve the model's quality-of-fit in future work would be to consider the limitation parameters $\tau_e$, $\omega_{nm}$ and $\zeta_{nm}$ as truly free, and participant-specific, parameters, as we did for only the human operator gains $K_p$ and $K_r$ in this paper.

In Step 3, we analyzed the model's sensitivity to some of its key parameter settings. To match the experiment data of [10], one of the key additions we propose for Hess' model from [6] is to include a human time delay $\tau_e$. Indeed, for matching our experiment data, we found that a delay of 0.2 s provided the best results, on average. Furthermore, we

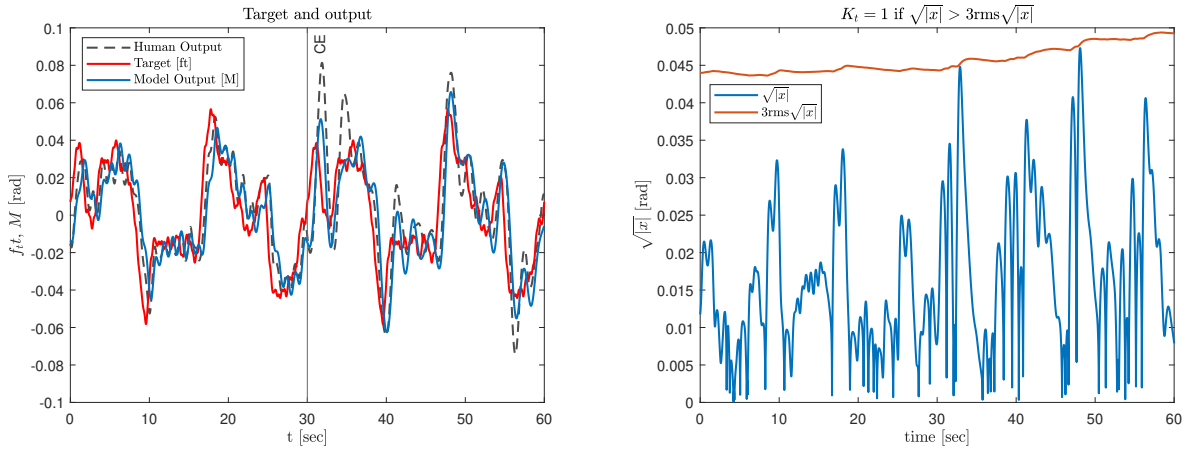


**(a) Tracking performance** **(b) Triggering logic**

**Fig. 17 Example of missed Triggering for condition DYN12 and a CE dynamics transition at 30 s: (a) tracking performance showing the forcing function $f_t$, modeled CE output $M$, and measured CE output from [10], (b) Triggering logic showing $\sqrt{|x|}$ and the Triggering limit ($3\text{rms}\sqrt{|x|}$).**

performed an analysis to investigate the effects of this added time delay on the adaptive Triggering and Adaptation mechanisms of the model. While the effect of the added delay was found to be small on the triggering, the fact that a delay directly results in larger (steady-state) tracking errors (and hence larger $x$ and $X_n$ signals) was found to strongly affect the strength of modeled gain adaptations. For this reason, we propose to include the 'adaptation constants' $K_{a_r}$ and $K_{a_p}$ as additional model parameters (proposed as constants of 1 and 0.35, respectively, in [6]), to enable tuning of the strength of the gain updates, and avoid over- and under-reaction of the model. We found that the values of these constants needed to be selected per participant, as for $K_r$ and $K_p$, to match the changes in both gains between each participants DYN1 and DYN2 data. In future work, it should be investigated if rather than adding these two additional independent tunable model parameters, the values of $K_{a_r}$ and $K_{a_p}$ may be determined based on (offline) analysis of reasonable post-transition tracking performance and open-loop stability.

Furthermore, in Step 3 we analyzed the required tuning of the different low-pass filters that are included in the model's adaptive logic to account for lags in human detection and parameter adjustments. In [7], three different second-order low-pass filters are applied: on the $x$-signal ($H(s)$), on the $X_n$ signal, and on the $\Delta K_r$ signal ($J(s)$). For $H(s)$, we found that the proposed break frequency of 1.5 rad/s [6] was too low to ensure Triggering of the model for our DYN12 condition, especially for participants who controlled with a low crossover frequency $\omega_c$. Hence, the $H(s)$ break frequency is a crucial tuning parameter for the model's adaptive logic, that likely will need to be adjusted for different CE-transition scenarios. In our analysis, we omitted the second low-pass filter on the $X_n$ signal, as it was found to be superfluous with the (same) filter also being applied again on the $\Delta K_r$ that is proportional to $X_n$, see Eq. (6). Finally, our analysis of how the break frequency of the $J(s)$ filter affected the model's tracking performance directly after the DYN12 CE transition showed that an unfiltered step-like adjustment in human operator gains is, in fact, optimal. While previous work also suggested near-instantaneous adjustment of human operator gains [7], the fact that the model's post-transition tracking performance was still found to be much worse than the real human operator data, indicates that further research is required to model this transient phase of a CE transition.

Finally, in Step 4 we performed validation of the adaptive pilot model for the data from all participants of [10] for the time-varying conditions DYN12 and DYN21. For DYN12, it was found that the model is able to capture the adaptive human behavior for the participants, if the Triggering mechanism of the model was activated. Furthermore, it was found that Triggering activation directly depends on the level of tracking performance and crossover frequency adopted in the pre-transition phase. For participants with a low-gain strategy (and comparatively large tracking errors) the Triggering mechanism was found to often not be activated. Overall, we conclude that the success of using the model depends directly on participants' (pre-transition) crossover frequencies, which should preferably be $\omega_c > 0.9$ rad/s. Furthermore, this analysis has shown that the experiment data from [10] included a number of participants with what can be considered a very low-gain strategy. Hence, to further aid our development of time-varying human control models

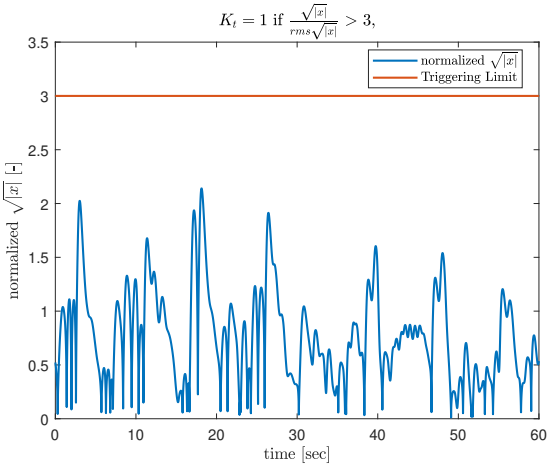


**Fig. 18 Example normalized $\sqrt{|x|}$ signal compared to the model's Triggering limit for DYN21, where the Triggering is not activated for the CE dynamics transition at 30 s.**

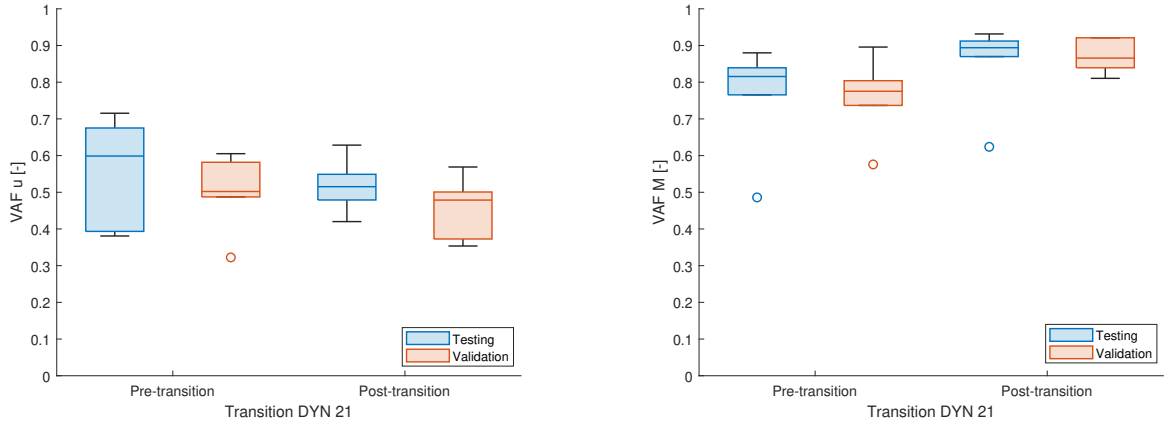


**(a) VAF$_u$** **(b) VAF$_M$**

**Fig. 19 Comparison of pre- and post-transition quality-of-fit for condition DYN21 for (a) VAF$_u$ and (b) VAF$_M$.**

for pursuit tracking tasks, in future work we aim to collect a second set of experiment data, for the same steady-state and time-varying scenarios, with better trained and more high-gain participants.

For condition DYN21, our Step 4 analysis showed the adaptive pilot model struggles to model the (for human operators less problematic) transition from controlling a double integrator (DYN2) to a single integrator (DYN1). This was anticipated, as other models, with similar adaptive mechanisms based on the detection of uncharacteristic larger tracking errors, have also shown difficulties in capturing such a transition [10]. As explained in [6], Hess' model was also not originally designed to model transitions that result in more easily controlled CE dynamics. Despite the fact that we see that VAF$_u$ values decrease by 8% on average for the post-transition phase in condition DYN21, the retained pre-transition control gain settings do not result in large post-transition tracking errors, and hence no Triggering and Adaptation by the model. This implies that a structural extension of the model's adaptive logic – e.g., not only triggering based on tracking errors, but also, for example, on changes in control activity or phase margin – is needed to also achieve its activation for CE transitions as considered here in condition DYN21.

## VI. Conclusion

In this paper, we present an analysis and validation effort for the 'adaptive pilot model' proposed by Hess [6] for modeling human operator time-varying dynamics in a pursuit tracking task. We used a set of recent human-in-the-loop

experiment data, with controlled element dynamics transitions from a single integrator to a double integrator and vice versa, to parameterize the model for 10 different participants and verify the effectiveness, and required tuning, of the model's adaptive Triggering and Adaptation mechanisms. For the considered controlled element dynamics transitions, it was found that a number of modifications and simplifications to the original model were required to achieve an accurate fit to the steady-state tracking data (e.g., adding a human operator delay) and to achieve realistic triggering of the adaptive logic in the time-varying conditions (e.g., removing/re-tuning the adaptive logic's different low-pass filters). Overall, the model was found to accurately predict human operator adaptation for controlled element transitions from a single to a double integrator, as the sudden degradation in tracking performance caused by this transition induces the model's Triggering logic to activate. The predicted gain adaptations were also found to be realistic, and improve the model's post-transition quality-of-fit by 30% compared to a non-adaptive model. However, the sensitivity of the model's Triggering logic was found to depend strongly on participants' pre-transition crossover frequency: the model's trigger activation was most reliable for the participants with the highest crossover frequencies (up to 1.5 rad/s) in our data set, but would not activate (even with model parameter updates) for participants with crossover frequencies below 0.9 rad/s. Finally, it was found that the model's adaptive logic could not predict the measured behavior adaptation for transitions from double to single integrator dynamics, for which the adaptive logic was not triggered, as this transition to more stable dynamics does not (negatively) impact tracking performance. Overall, we conclude that the modeling framework's adaptive logic is a promising, but somewhat limited, representation of how human operators may adapt to changes in controlled system dynamics, and that more experiments are required to successfully include all relevant mechanisms of humans' adaptive manual control behavior.



## Acknowledgments

We would like to express our gratitude to Prof. Ronald Hess for his instrumental help and willingness to answer our many questions while realizing our implementation of his adaptive pilot model.

## References

[1] Young, L.R., Green, D.M., Elkind, J.I., Kelly, J.A., "Adaptive Dynamic Response Characteristics of the Human Operator in Simple Manual Control," *IEEE Transactions on Human Factors in Electronics*, Vol. HFE-5, No. 1, 1964, pp. 6–13. https://doi.org/10.1109/THFE.1964.231648.

[2] Miller, D.C. and Elkind, J.I., "The adaptive response of the human controller to sudden changes in controlled process dynamics," *IEEE Transactions on Human Factors in Electronics*, , No. 3, 1967, pp. 218–223.

[3] Phatak, A.V. and Bekey, G.A., "Model of the Adaptive Behavior of the Human Operator in Response to a Sudden Change in the Control Situation," *IEEE Transactions on Man-Machine Systems*, Vol. 10, No. 3, 1969, pp. 72–80. https://doi.org/10.1109/TMMS.1969.299886.

[4] Young, L. R., "On Adaptive Manual Control," *Ergonomics*, Vol. 12, No. 4, 1969, pp. 635–674. https://doi.org/10.1080/00140136908931083.

[5] Hess, R. A., "Modeling Pilot Detection of Time-Varying Aircraft Dynamics," *Journal of Aircraft*, Vol. 49, No. 6, 2012, pp. 2100–2104. https://doi.org/10.2514/1.C031805.

[6] Hess, R.A., "Modeling human pilot adaptation to flight control anomalies and changing task demands," *Journal of Guidance, Control, and Dynamics*, Vol. 39, No. 3, 2016, pp. 655–666.

[7] Zaal, P. M. T., "Manual Control Adaptation to Changing Vehicle Dynamics in Roll–Pitch Control Tasks," *Journal of Guidance, Control, and Dynamics*, Vol. 39, No. 5, 2016, pp. 1046–1058. https://doi.org/10.2514/1.G001592.

[8] Mulder, M., Pool, D. M., Abbink, D. A., Boer, E. R., Zaal, P. M. T., Drop, F. M., Van der El, K., and Van Paassen, M. M., "Manual Control Cybernetics: State-of-the-Art and Current Trends," *IEEE Transactions on Human-Machine Systems*, Vol. 48, No. 5, 2018, pp. 468–485. https://doi.org/10.1109/THMS.2017.2761342.

[9] Tohidi, S.S. and Yildiz, Y., "Adaptive human pilot model for uncertain systems," *Proceedings of the 18th European Control Conference (ECC)*, 2019, pp. 2938–2943. https://doi.org/10.23919/ECC.2019.8795847.

[10] Terenzi, L., Zaal, P. M. T., Pool, D. M., and Mulder, M., "Adaptive Manual Control: a Predictive Coding Approach," *Proceedings of the AIAA SciTech Forum, San Diego (CA), 2022*, 2022. https://doi.org/10.2514/6.2022-2448.

[11] Young, L.R., "On adaptive manual control," *Ergonomics*, Vol. 12, No. 4, 1969, pp. 635–674.

[12] Hess, R.A., "Modeling pilot control behavior with sudden changes in vehicle dynamics," *Journal of Aircraft*, Vol. 46, No. 5, 2009, pp. 1584–1592. https://doi.org/10.2514/1.41215.

[13] Hess, R.A., "A model for pilot control behavior in analyzing potential loss-of-control events," *Proceedings of the Institution of Mechanical Engineers, Part G: Journal of Aerospace Engineering*, Vol. 228, No. 10, 2014, pp. 1845–1856. 10.1177/0954410014531218.

[14] Popovici, A., Zaal, P. M. T., and Pool, D. M., "Dual Extended Kalman Filter for the Identification of Time-Varying Human Manual Control Behavior," *Proceedings of the AIAA Modeling and Simulation Technologies Conference, Denver (CO)*, 2017. https://doi.org/10.2514/6.2017-3666.

[15] Van Grootheest, A., Pool, D. M., Van Paassen, M. M., and Mulder, M., "Identification of Time-Varying Manual Control Adaptations with Recursive ARX Models," *Proceedings of the AIAA Modeling and Simulation Technologies Conference, Kissimmee (FL)*, 2018. https://doi.org/10.2514/6.2018-0118.

[16] Plaetinck, W., Pool, D. M., Van Paassen, M. M., and Mulder, M., "Online Identification of Pilot Adaptation to Sudden Degradations in Vehicle Stability," *Proceedings of the 2nd IFAC Conference on Cyber-Physical & Human-Systems, Miami (FL)*, IFAC-PapersOnLine, Vol. 51, 2019, pp. 347–352. https://doi.org/10.1016/j.ifacol.2019.01.020.

[17] McRuer, D.T. and Jex, H.R., "A review of quasi-linear pilot models," *IEEE Transactions on Human Factors in Electronics*, , No. 3, 1967, pp. 231–249. https://doi.org/10.2514/6.2010-8092.

[18] Van Ham, D. M., Jacomijn M.and Pool, and Mulder, M., "Predicting Human Control Adaptation from Statistical Variations in Tracking Error and Error Rate," *IFAC-PapersOnLine*, Vol. 55, 2022, pp. 166–171. https://doi.org/10.1016/j.ifacol.2022.10.250.

[19] Jakimovska, N., "Adaptive Manual Control: Detection of Human Adaptation to Sudden Changes in Controlled Element Dynamics," Master's thesis, TU Delft, Faculty of Aerospace Engineering, 2022. URL http://resolver.tudelft.nl/uuid:448d4ac9-12b2-4002-b590-a9830c0470a5.

[20] Hess, R.A., "Effects of time delays on systems subject to manual control," *Journal of Guidance, Control, and Dynamics*, Vol. 7, No. 4, 1984, pp. 416–421. https://doi.org/10.2514/3.56380.

[21] Zollner, H., Pool, D. M., J., D. H., Van Paassen, M. M., and Mulder, M., "The effects of controlled element break frequency on pilot dynamics during compensatory target-following," *AIAA Modeling and Simulation Technologies Conference*, 2010. https://doi.org/10.2514/6.2010-8092.